

Final Report

Project Title: Three-dimensional minority carrier lifetime mapping of thin film semiconductors for solar cell applications

Project Period: 10/01/2012 – 09/30/2015

Project Budget: \$450,000

Submission Date: 1/15/2015

Recipient: PLANT PV Inc.

Address: 3707 Naughton Ave
Belmont CA 94002

Award Number: DE-EE0005953

Project Team: PLANT PV Inc. / Molecular Foundry LBNL

Contacts: Brian Hardin
Co-Founder PLANT PV
Phone: (650) 814-0594
Email: bhardin@plantpv.com

Executive Summary

This project addresses the difficulty of accurately measuring charge carrier dynamics in novel semiconductor materials for thin film photovoltaic cells. We have developed a two-photon lifetime tomography technique to separate bulk minority carrier lifetime from surface recombination effects and effects of recombination at sub-surface defects. This technique also enables us to characterize how local defects such as grain boundaries—buried below the surface of a sample—affect carrier lifetimes in the active layer, dynamics that have been previously inaccessible.

We have applied this newly developed technique to illuminate how CdCl_2 treatment improves CdTe PV efficiency. From striking 3D lifetime tomography maps, a clear, sub-surface understanding emerges of the photophysical changes that occur in CdTe active medium following exposure to CdCl_2 , a standard step in the fabrication of high-efficiency CdTe-based solar cells.

This work demonstrates a well-defined method to quantify grain-boundary, interface, and bulk recombination in CdTe and other optically-active polycrystalline semiconductor materials; information that can provide critical information to the development of next-generation photovoltaics and many other semiconductor technologies.

Table of Contents

Executive Summary	2
Table of Contents	3
Background	4
Introduction.....	6
Technical Work Summary.....	7
Budget Period 1: Technique development and validation	7
Go/No-Go Decision Point.....	9
Budget Period 2: Thin film PV studies and technique advancement.....	9
Project Results and Discussion	11
Task 1: Construction and validation of a depth profiling 2P-TRPL microscope.....	11
Task 2 Measure surface recombination velocity and bulk minority carrier lifetime.....	12
Subtasks 2.1/2.2: 1P- and depth-of-focus 2P-TRPL on single crystal CdTe.....	12
Subtask 2.3 Modelling of 2P-TRPL carrier dynamics.....	13
Subtask 2.4 Extract SRV and lifetime from 2P-TRPL measurements.....	16
Task 3: Three Dimensional Lifetime Tomography	17
Subtask 3.1.1 Integration of 3D scanning	17
Subtasks 3.1.2 and 3.1.3 Lateral resolution measurements	18
Subtask 3.2: 3D 2P-TRPL of CdSe	19
Additional 3D measurements on CdTe poly-crystalline materials	21
Task 4 Two-photon laser-beam induced current (2PIC).....	22
Subtask 4.1: 2PIC capability build out.....	22
Subtask 4.2 Depth-of-Focus 2PIC on CZTS solar cells	22
Task 5. Two Photon characterization and defect analysis of CdTe PV	25
2P-TRPL analysis of isolated grain boundaries in CdTe bi-crystals.....	25
Initial CdTe poly-crystal thin film 2P-TRPL measurements	27
Lifetime at Grain Boundaries in CdTe polycrystalline films	28
Effects of CdCl ₂ processing on grain boundaries in CdTe polycrystalline films	29
Task 6 Microscope depth resolution improvement	35
Two-photon solid immersion microscopy	35
Deconvolution Techniques	38
Oil Immersion microscopy yields 1µm nominal depth resolution	39
Conclusions	40
Budget and Schedule	41
Path Forward	42
References	42

Background

Achieving the SunShot goal of 25% efficient photovoltaic cell (PV) modules at a cost of \$0.50/W will likely require thorough studies of novel, photoactive semiconductors. One of the greatest challenges of evaluating unconventional semiconductor materials for PV applications is accurately measuring the bulk minority carrier lifetime. The minority carrier lifetime is considered the most critical and variable parameter in photovoltaic materials.¹ Well-established photoconductivity techniques (e.g. Quasi-Steady State Photoconductivity) are often used to determine the minority carrier lifetime for indirect band gap materials that have long minority carrier lifetimes between 20 μ s and 1 ms, such as silicon. However, these techniques are not effective at measuring short minority carrier lifetimes of direct band gap materials, which are typically less than 100 ns, or materials that have many traps and low doping levels.¹ For direct band gap materials, optical techniques such as linear time-resolved photoluminescence (TRPL) are often used to estimate the minority carrier lifetime.²

In the linear TRPL system, a short laser pulse (e.g. 100 fs) consisting of photons above the band gap of the semiconductor is absorbed by the semiconductor, generating excess carriers. A fraction of these carriers radiatively recombine, emitting photons that are detected by a time-correlated single photon counting system. The characteristic time over which the carriers recombine can then be related to the minority carrier lifetime. In these measurements the majority of photons are absorbed within 100-500 nm of the semiconductor surface as shown in Fig 1 because the incident photons have energies above the band gap. Linear TRPL studies can thus be highly influenced by surface recombination. For material systems with low surface recombination velocities (SRV), the bulk minority carrier lifetime can be determined by measuring a mono-exponential TRPL decay, while systems with large SRV exhibit decays dominated by surface effects. As an example, NREL recently demonstrated that linear TRPL of freshly deposited, high quality CIGS thin films exhibited mono-exponential behavior resulting in a minority carrier lifetime greater 250 ns.³ However, when left in air for 24 hours the surface recombination velocity drastically increased and the resulting TRPL showed a steep decline, resulting in lifetimes of less than five nanoseconds.³ For many well-studied semiconductors (e.g. GaAs and CIGS) the research community has established surface passivation techniques⁴ to significantly reduce the surface recombination velocity and directly measure minority carrier lifetimes⁵. However, linear TRPL of novel materials often results in multi-exponential TRPL decay where surface recombination plays an important role. The convolution of surface and bulk recombination processes then prevents an accurate determination of the bulk minority carrier lifetime of new PV material systems.

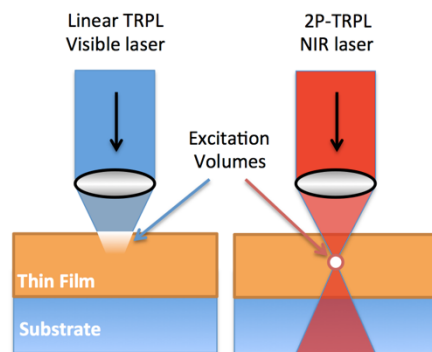


Figure 1. (Left) In linear (1P) TRPL, incident photons are above the band gap and produce an exponential excess carrier concentration profile that follows Beer’s law. (Right) In the two-photon (2P) excitation process, incident photons are below the band gap and require higher photon flux at the focal point (white circle) for non-linear processes to excite excess carriers.

In addition to surface recombination interfering with measurement of bulk carrier lifetime, heterogeneity in local lifetime can be important to understand when optimizing PV materials. Polycrystalline PV films are generally rapidly deposited, resulting in grain sizes that are commensurate with the film thickness which is typically just several microns. In addition, the $p-n$ junction is formed using a layer that is often lattice mismatched and produces a highly defective interface. As a result, adverse (non-radiative) carrier recombination at this interface, at grain boundaries, and in the inhomogeneous bulk critically impacts aggregate lifetime and performance. However, there has not been a well-defined method to quantify grain-boundary, interface, and bulk recombination in these semiconductor materials. Not having this information makes it difficult for researchers to identify the key recombination mechanisms and to monitor how processing affects such carrier dynamics. This forces empiricism and conjecture in lieu of scientific results. Here we extract this information *in-situ* with high-resolution using two-photon lifetime tomography. This technique allows 3D mapping of carrier lifetimes throughout the film, as we show here for the first time.

The two-photon 3D lifetime tomography is applied to CdTe solar cells where a CdCl₂ treatment step is used to significantly improve device performance^{6,7}. This treatment has been shown to induce two changes in the CdTe active layer: (1) recrystallization and grain coalescence of the CdTe film^{8,9} and (2) preferential Cl concentration at the grain boundaries that has been suggested to passivate grain boundary recombination¹⁰. These changes involving grain boundaries have been theorized to be the cause for increased cell performance^{10–12}, but direct evidence of the improvement of optoelectronic properties at grain boundaries has not yet been shown. In this work, novel three-dimensional lifetime tomography reveals that the CdCl₂ treatment not only improves carrier lifetimes throughout the film, but also strongly improves carrier lifetime at grain boundaries and interfaces (including the surface and the $p-n$ junction), leaving the film with a much longer local carrier lifetime distribution.

Introduction

For this project, the PLANT PV/Molecular Foundry (PLANT PV/MF) team has developed innovative two-photon optoelectronic characterization techniques in order to decouple bulk and surface recombination, sub-surface defect recombination. This will enable a more accurate determination of the bulk minority carrier lifetime of novel photovoltaic materials and accelerate research and development efforts to achieve SunShot goals. Two-photon microscopy has been well used for biological applications¹³ and in a few cases for semiconductor characterization.^{14,15} However, this technique has never before been applied to PV material characterization. Two-photon absorption measurements^{14,16–18} use photons with energies below the band gap to excite carriers in the semiconductor via a non-linear optical process. Efficient multi-photon excitation requires nearly simultaneous absorption of multiple photons and exhibits a nonlinear dependence on excitation density. Therefore, using a confocal microscope, it is possible to confine the excitation to a sub-surface diffraction-limited volume. As is shown schematically in Fig. 2a, we can move this excitation volume throughout the film to form complete 3D carrier lifetime map and photoluminescence (PL) intensity maps by adjusting the focal depth and x-y positions of the laser and the sample. Using two-photon absorption as the excitation source thus allows the independent examination of the front surface, bulk, and buried interfaces of thin films. Furthermore, by decoupling bulk and surface effects, this technique enables an accurate measurement of the bulk minority carrier lifetime, as described in the following paragraph.

Two-photon excitation can be applied with Time-Resolved Photoluminescence (2P-TRPL) to measure the minority carrier lifetime inside the semiconductor. It is possible to perform depth-of-focus 2P-TRPL to vary the excitation in the film and independently determine both the surface recombination velocity and the bulk minority carrier lifetime of novel photoactive materials [see **Task 1** and **2**]. 2P-TRPL will allow researchers to quickly ascertain if new materials and morphologies have the requisite lifetimes without having to develop surface passivation techniques and, importantly, without having to fabricate complete electronic devices. Once materials with sufficient optoelectronic properties have been incorporated into complete devices it is possible to then use two-photon absorption to excite charges at different depths within the device and collect current in a technique we call two-photon induced current (2PIC). This technique has been shown to provide high-resolution measurements of buried Si devices¹⁵. Depth-of-focus 2PIC may be able to study the impact of inhomogeneous films and buried interfaces on charge collection efficiency, both of which are inaccessible with linear TRPL techniques. In addition, 2PIC can be performed under different voltage biases providing insight into localized regions of energetic traps throughout the film thickness. The technique thus may be particularly relevant to study buried interfaces and graded band gap thin films such as CIGS.

Three-dimensional (3D) tomographic maps can be created by performing depth-of-focus experiments while scanning the sample position with an x-y stage. Three-dimensional 2P-TRPL provide detailed tomographic maps of the minority carrier lifetime on both incomplete [**Task 3**] and completed [**Task 4**] solar cells. Three-dimensional 2PIC [**Task 4**] will provide tomographic maps of charge collection efficiency that can be taken

simultaneously with 2P-TRPL. Variation in the minority carrier lifetime [Task 3] can then be used to identify and study defective portions of the thin film more closely [Task 5].

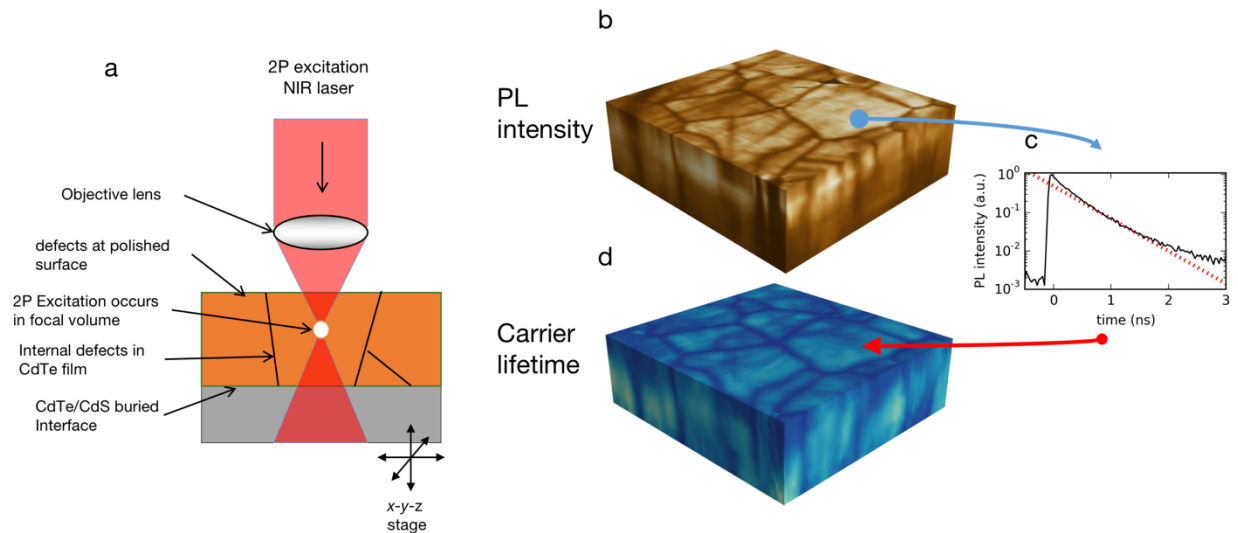


Figure 2. 3D 2P-TRPL microscopy of CdTe thin films. a) Schematic of 2P-TRPL microscopy measurements. (b) a representative 3D data cube of PL intensity data acquired with 2P-TRPL microscopy. (c) At each data point we acquire a lifetime trace and fit data to exponential decay dynamics and to a 3D lifetime data cube in (d).

Technical Work Summary

Budget Period 1: Technique development and validation

Task 1. Construction and validation of a depth profiling 2P-TRPL microscope

In this task we constructed a microscope that will allow for 2P-TRPL measurements. We will then use the microscope to measure bulk lifetimes of single crystal materials (CdTe as our model system). With these material systems, surface recombination is minimized and will not strongly affect lifetime measurements. Thus we demonstrate that 2P-TRPL can produce the same results as traditional TRPL for these known systems.

Subtask 1.1: 2P-TRPL Microscope Build out and Depth Scanning tests

Subtask 1.2: Validating 2P-TRPL Measurements of Bulk Lifetime

We performed 2P-TRPL on the same CdTe samples using excitation wavelengths ranging from 800-1500 nm and average power ranging from 5-800 mW and measure

the resulting emission spectrum and PL decay. By measuring an extensive range of wavelengths and incident photon fluxes we will determine the acceptable wavelengths and power ranges to achieve similar PL decay results versus linear TRPL.

During Task 1 we achieved the following milestones:

- Time-resolved collection of two-photon PL with 100 ps time resolution and 2.0 μm depth resolution. Our original goal of 1.0 μm depth resolution was not achieved for this task until later during Task 6 where we developed resolution-improvement techniques to achieve 1.0 μm depth nominal depth resolution.
- Extract bulk minority carrier lifetimes using 2P-TRPL that are within a factor of 2 compared with lifetimes measured using linear TRPL on the model CdTe system averaged over multiple samples. Repeated lifetime measurements of the same location / sample will have a $\leq 20\%$ standard deviation.

Task 2. Measure Surface recombination velocity (SRV) and Bulk Minority Carrier Lifetime

The key goal in Task 2 was to measure surface recombination velocity (SRV) and bulk minority carrier lifetime of a model system. This involved measuring a single crystal CdTe using 1P- and 2P-TRPL (sub tasks 2.1, 2.2) and developing a physical model (subtask 2.3) to extract bulk minority carrier lifetime and surface recombination velocity from the CdTe sample (subtask 2.4). Within the year of the project start we published a paper¹⁶ in Nature's *Scientific Reports* based on the Task 1 and the results as of subtask 2.2.

Task 2 Sub Tasks:

- 2.1 Improve bulk lifetime of CdTe sample using Cd overpressure anneal
- 2.2 Perform linear TRPL to improve bulk lifetime of CdTe. Perform depth-of-focus 2P-TRPL with the expectation that the PL decay will vary with excitation depth.
- 2.3 Further develop a 1D physical rate model to include a generation profile that closely matches that produced by two-photon excitation inside the semiconductor.
- 2.4 Fit 2P-TRPL data to rate model in order to extract SRV and the bulk minority carrier lifetime. Compare the independently modeled bulk minority carrier lifetime with the minority carrier lifetime measured in the model CdTe crystal.

We successfully achieved the Task 2 Milestone:

Independently extract SRV and bulk minority carrier lifetime of CdTe system using 2P-TRPL.

Task 3. Three Dimensional Lifetime Tomography

In this task we extend the 2P-TRPL technique to produce 3D tomographic maps of lifetimes in single crystal semiconductors.

- *Task 3.1: Integrate 3D 2P-TRPL System and Determine Lateral Resolution*
- *Task 3.2: 3D 2P-TRPL of CdSe thin Films*

We achieved the Task 3 Milestone:

3D tomographic lifetime map of patterned buried InGaN quantum well structures and CdSe thin films with $0.5 \times 0.5 \mu\text{m}^2$ lateral resolution and $1 \mu\text{m}$ depth resolution. Repeated lifetime measurements of the same location / sample will have a $\leq 20\%$ standard deviation. Again depth resolution was limited, but was addressed in Task 6.

Go/No-Go Decision Point

Four key milestones were part of the Go/No-Go decision.

- 1) Extract bulk minority carrier lifetimes using 2P-TRPL that are within a factor of 2 compared with lifetimes measured using linear TRPL on the model CdTe system averaged over 20 measurements. Repeatability of identical lifetime experiment will have a $\leq 20\%$ standard deviation.
- 2) Depth resolution $\leq 1 \mu\text{m}$ verified with the model QW system.
- 3) Three-dimensional 2P-TRPL scanning capabilities with 500 nm lateral resolution over a $75 \times 75 \mu\text{m}$ area.
- 4) It is preferable that depth-of-focus 2P-TRPL can separate SRV and bulk minority carrier lifetimes but it may not be required to get an accurate interpretation of the dominant recombination mechanisms in thin films.

All these milestones were achieved at the time of the Go/No-Go decision point, with the exception of the $1 \mu\text{m}$ depth resolution. During discussions at the time of the decision, we added Task 6 to successfully address this.

Budget Period 2: Thin film PV studies and technique advancement

Task 4. Two-Photon Induced Current (2PIC) Measurement on CZTS Solar Cells

In Task 4 we developed the two-photon induced current technique. With this technique we measure completed solar cells to study the charge collection efficiency inside the thin films of conventional CIGS.

- *Subtask 4.1: 2PIC capability build out*
- *Subtask 4.2: Depth-of-Focus 2PIC on CdTe or CZTS solar cells*

The Task 4 milestone was successfully completed:

- Simultaneous overlaid 3D 2P-TRPL and 2PIC tomography maps of CdTe or CZTS solar cells over 75x75 μ m area, through the depth of the film. Lateral resolution will be 500 nm and depth resolution will be 2 μ m.

Task 5. Two Photon Characterization and Defect Analysis of CdTe/CZTS PV

The 2P-TRPL method developed in the previous tasks is now applied to a specific industrially-relevant material system in Task 5. In this task we have used the high-resolution 3D probing of carrier lifetime to characterize the optoelectronic behavior of buried grain boundaries and other defects in CdTe films. We have developed two different collaborations on this material system, and are currently preparing a manuscript for a peer-reviewed submission.

- *Subtask 5.1:* 3D minority carrier lifetime and photocurrent maps of CdTe thin films of varying morphologies
- *Subtask 5.2:* Defect and Interface analysis of CdTe PV

We have successfully completed this Task 5 milestone:

Defect and Interface analysis of CdTe PV materials. Use 2P-TRPL to measure optoelectronic properties at defects and interfaces.

Task 6. Solid Immersion Lens development for microscope depth resolution improvement

- Subtask 6.0 (Q7-8) Initial tests of a ZnSe solid immersion lens (SIL) on a reference sample without integration apparatus.
- Subtask 6.1 (Q9-10): Design, build and test solid immersion lens (SIL) integration apparatus
- Subtask 6.2 (Q11): Test depth resolution on CdTe solar cell by creating 2P-TRPL/2PIC map with SIL system.
- Task 6 Milestone (Q10): <1 μ m depth resolution of 2P-TRPL using solid immersion lens without integration apparatus.
- Task 6 Milestone (Q12): <1 μ m depth resolution of 2P-TRPL using solid immersion lens system

We have successfully completed the following final milestones:

- Confocal microscope/NIR laser system capable of performing 2P-TRPL and 2PIC with ≤ 1 μ m depth resolution and 500 nm lateral resolution over a 75 x 75 μ m area.
- Demonstrate measurement of bulk minority carrier lifetime and surface recombination velocity of an unpassivated thin film (CdTe) using 2P-TRPL.

Show that linear TRPL cannot measure bulk minority carrier lifetime in this sample.

- Software to extract SRV and bulk lifetime from 3D 2P-TRPL measurements.
- 3D minority carrier lifetime and 3D 2PIC maps of CdTe or CZTS thin film solar cells (four different 75 x 75 μm regions on the solar cell) Repeated lifetime measurements of the same location / sample will have a $\leq 20\%$ standard deviation.

Project Results and Discussion

Task 1: Construction and validation of a depth profiling 2P-TRPL microscope

Our first task was to build the 2-P TRPL microscope with capabilities of scanning both laterally and in depth. This allows us to measure two-dimensional spectral as well as carrier lifetime maps of photovoltaic cell materials. A schematic of the 2P-TRPL microscope is shown in Figure T1.1a. We coupled a coherent Mira 900 Ti:Sapphire excitation laser (700-1000 nm tunable, 150 fs pulse duration, 80MHz) to the input of a Nikon Eclipse Ti-U microscope with a Nikon 100x NA=0.95 NA objective to photoexcite the sample. An optical parametric oscillator (OPO) with an optional doubling crystal enables tuning of the laser to an even larger range. We have incorporated into the microscope a three axis MadCityLabs NanoPDQ piezo nanopositioning sample stage with 75 x 75 μm mapping capabilities and 1 nm step precision. The depth scanning ability allows us to study how the carrier lifetime varies with depth into the sample, enabling the separate determination of the bulk recombination lifetime and surface recombination velocity. The lateral scanning ability allows studies of how the morphology of polycrystalline films affects the minority carrier lifetime and also to observe how homogenous the lifetime is in polycrystalline films. Photoluminescence is collected through a 150 μm pinhole and into detection optics. For spectral collection we used an Acton 2300i spectrometer with 150 grooves/mm grating and an Andor iXon electron-multiplied CCD. For time-resolved collection we first spectrally-filter the PL using band pass filters and then detect the PL with a single-photon avalanche diode (Micro Photon Devices PDM series). A PicoQuant PicoHarp 300 time-correlated single-photon counting (TCSPC) system is used to record the timing data. The 2-P TRPL microscope can easily be changed into a 1-P TRPL by converting the laser excitation to a shorter wavelength using a frequency doubling crystal.

To verify that we are achieving 2P absorption in each of our test samples, we measure the photoluminescence intensity as a function of the excitation intensity. As a model system, we measured the PL intensity dependence for solutions of the organic dye Rhodamine 101 in ethanol, which is known to have a PL quantum efficiency of nearly 100%. When excited with below bandgap light ($\lambda=830\text{nm}$), the photoluminescence intensity was proportional to the square of the laser fluence (power law of 1.93). Conversely, when excited by above bandgap light, the photoluminescence intensity was linearly proportional to the fluence (power law of 1.05) (see Fig. T1.1b). We have written

software in python to automate the process of scanning in one, two, or three dimensions and collecting the photoluminescence spectrum or TRPL transient at each point. We have also written software in python to extract bi-exponential decay lifetimes from the TRPL data to generate lifetime maps.

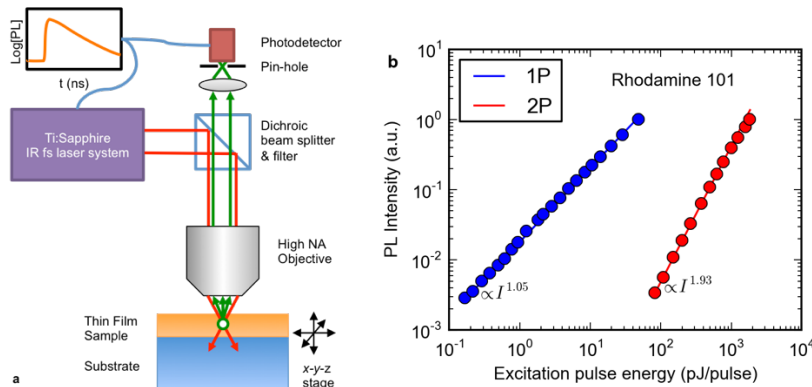


Figure T1.1 (a) Schematic of the 2P-TRPL microscope used in this study. (b) One-photon and two-photon PL intensity dependence of Rhodamine 101 in ethanol with power-law fits.

Task 2 Measure surface recombination velocity and bulk minority carrier lifetime

The key goal in Task 2 was to measure surface recombination velocity (SRV) and bulk minority carrier lifetime of a model system. This involved measuring a single crystal CdTe using 1P- and 2P-TRPL (sub tasks 2.1, 2.2) and developing a physical model (subtask 2.3) to extract bulk minority carrier lifetime and surface recombination velocity from the CdTe sample (subtask 2.4). Within the year of the project start we published a paper¹⁶ in Nature's *Scientific Reports* based on the Task 1 and the results as of subtask 2.2.

Subtasks 2.1/2.2: 1P- and depth-of-focus 2P-TRPL on single crystal CdTe

Depth-of-focus 2P-TRPL, shown in Fig. T2.1, was performed on an annealed CdTe crystal and revealed a $>10x$ increase in the bulk lifetime over an as-deposited sample. The resulting components of the biexponential fit of the lifetime curves are shown in Fig T2.1b (fast) and Fig. T2.1c (slow component). The weightings for the fast and slow components are shown in Fig. T2.1d and reveal a clear transition from short, surface-dominated to long, bulk-dominated recombination dynamics. This clear transition was not observed in the sample prior to this Cd treatment. The weighting for the slow component in the bulk approaches unity, indicating there is now a single dominant decay pathway in the bulk that results in a monoexponential decay.

At the surface, the 2P TRPL decay of the treated CdTe crystal is dominated by a fast component with a lifetime of 0.23 ns, which is similar to the fast component before treatment. This suggests that the treatment left the surface unimproved. There is however a small contribution of a 9 ns slow component, which is much longer than the untreated sample's 0.7 ns. At a nominal focus depth of 1 μm we find that the fast

($\tau_f = 0.45$ ns) and slow ($\tau_s = 17.6$ ns) components are equally weighted. Deeper in the sample, the slow component dominates and reaches a $\tau_s = 73.0$ ns at a nominal focus depth of $3.4 \mu\text{m}$. At depths below this we note a continued increase in lifetime but we are originally unable to quantify this due to a limited 12 ns time window defined by the laser repetition rate. The slow components in these measurements are an order-of-magnitude longer than the equivalent measurements done on the untreated sample, indicating an improvement in bulk carrier lifetime due to the Cd treatment. (We were later able to use a laser pulse picker to measure a larger time window to more accurately measure the long lifetime component. See the section on subtask 2.4 later in this report.)

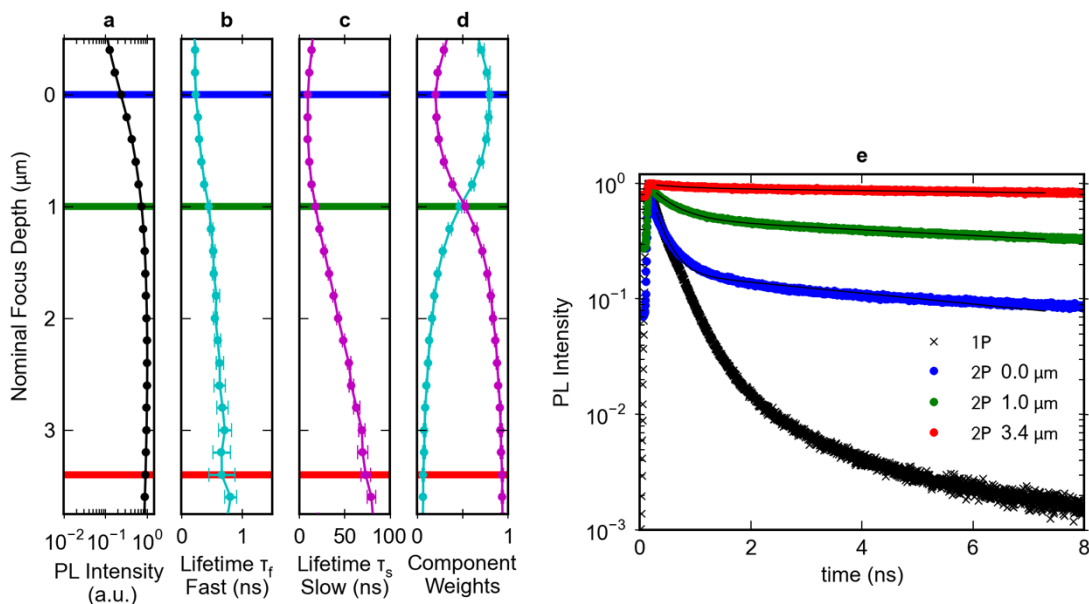


Figure T2.1 Depth-of-Focus two-photon TRPL of the treated CdTe crystal. (a) Total photoluminescence intensity as a function of nominal focus depth (Δz) into sample as measured by the motion of the sample stage. (b,c) Results of a biexponential fit of PL decay as a function of nominal focus depth into the sample. (b) Short and (c) long lifetime components of the biexponential fit. (d) Relative weights of short (cyan) and long (magenta) components of the biexponential fits. (e) Representative 2P-TRPL decay time traces at three different depths: at the surface and at nominal focus depths of $1.0 \mu\text{m}$ and $3.4 \mu\text{m}$. 1P-TRPL decay time trace is also plotted.

Subtask 2.3 Modelling of 2P-TRPL carrier dynamics

In order to extract physical quantities out of the data acquired in subtask 2.2 we have developed a computational analysis tool in subtask 2.3. We evaluated several algorithms for simulating the TRPL experiment and have developed a two-step model that enables the determination of the bulk recombination lifetime and surface

recombination velocity by fitting experimental 2P-TRPL data. A summary of the computational model that we have implemented is depicted in Figure T2.2.

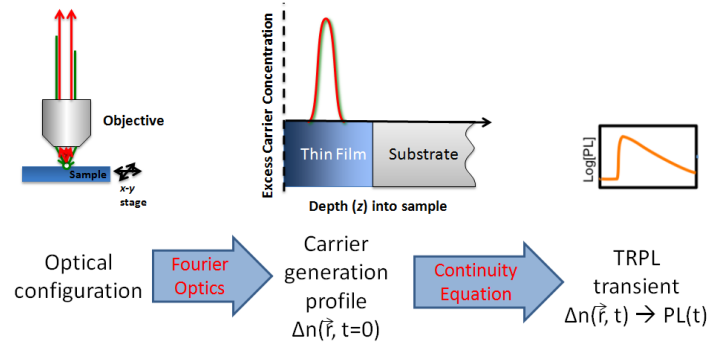


Figure T2.2. Summary of the 2-step simulation model to extract the bulk recombination lifetime and surface recombination velocity.

In the first step, the initial photo-generated excess carrier concentration from the laser pulse is calculated as a function of the position in the device using an optical model based on vectorial Fourier optics. The inputs to the model are the details of the geometry of the microscope, including the numerical aperture (NA) of the objective lens, the focal depth of the sample stage, as well as the index of refraction of the sample and surrounding medium (usually air), and excitation and emission wavelengths and 1-photon and 2-photon absorption coefficients. The optical model that we have selected by van de Nes¹⁹ uses a transfer matrix algorithm to account for reflection and refraction at material interfaces in determining the electromagnetic field intensity. Notably, the model can account for refraction that occurs at the top of the photovoltaic material sample that results in significant aberrations of the focal volume. We can then calculate the profile of excess carriers, n , generated from the simulated electric field profile $E(\mathbf{r})$ for both 1-photon and 2-photon excitation

$$n(\mathbf{r}, t = 0) = \frac{\lambda_{ex}}{hc} \left(\alpha \frac{cn_1 \epsilon_0}{2} E(\mathbf{r})^2 + \beta \left(\frac{cn_1 \epsilon_0}{2} E(\mathbf{r})^2 \right)^2 \right)$$

where α and β are the 1-photon and 2-photon absorption coefficients, respectively, and n_1 is the index of refraction of the material and λ_{ex} is the excitation wavelength.

In the second step of the simulation, we allow the excess minority carriers to diffuse and recombine according to the continuity equation, with the initial condition determined by the generation profile calculated from the optical simulations. The 1-D version of the continuity equation, including a bulk minority carrier recombination lifetime of τ is given below.

$$\frac{dn}{dt} = D \frac{d^2 n}{dz^2} - \frac{n}{\tau}$$

We have also performed simulations of the continuity equation in 3D and have found that the final simulated TRPL transients are similar to those produced by the 1D simulations for samples that do not have lateral variations. The surface recombination velocity factors into the boundary conditions, where v_1 and v_2 are the surface recombination velocities at the incident and back surfaces of the photovoltaic material of thickness d .

$$D \frac{dn}{dz} \Big|_{z=0} = n(z=0, t) v_1 \quad \text{and} \quad -D \frac{dn}{dz} \Big|_{z=d} = n(z=d, t) v_2$$

We first tried solving the diffusion equation by using a finite difference time domain (FDTD) algorithm to discretize the differential equations. We found that the FDTD method had stability problems when large values of the surface recombination velocity were used. The simulations would converge slowly, often requiring a minute or more for a simulation with a single set of parameters, which is too slow for an optimization routine.

We have since implemented a continuity-equation solver that uses a separation of variables expansion to converge upon the excess carrier evolution profile solution. This approach has been used by other solar cell researchers to extract surface recombination velocities from surface transient measurements, including recently by Ahrenkiel and Johnston²⁰. In this approach, we use a series expansion of excess carriers of the form:

$$n(z, t) = e^{-t/\tau} \sum_{i=0}^{\infty} (a_i \cos(\alpha_i) + b_i \sin(\alpha_i z)) e^{-\beta_i t}$$

This converts the differential equations and boundary conditions into a system of equations that can be solved numerically. We have found that 50 terms in the summation is generally more than sufficient for convergence and the simulations take only a few seconds on a standard laptop. Finally, the PL transient can then be calculated from the excess carrier profile.

$$PL(t) \sim \int_{z=0}^d n(z, t) e^{-\alpha(\lambda_{em})z} dz$$

This formula allows us to account for reabsorption of emitted light by the material.

We have developed an interactive user interface that allows us to explore the effects of optical and semiconductor parameters on PL decay time traces. As shown in Fig T2.3, we can enter optical excitation and collection parameters, including wavelength, absorption coefficients and stage position. Additionally, semiconductor parameters including ambipolar diffusivity, SRV and bulk lifetime can be explored. We plot simulated TRPL transients (upper right) as well as animated spatial distributions of carriers in the simulated sample (lower right).

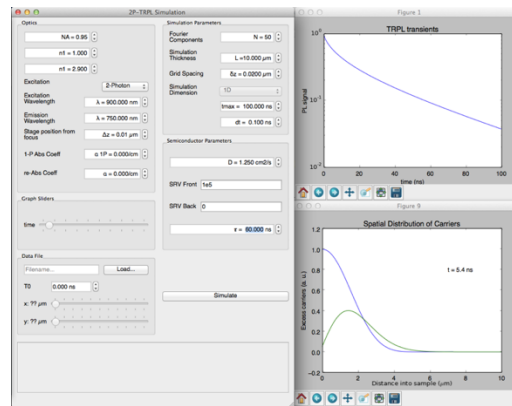


Figure T2.3. Graphical user interface to 2P-TRPL simulation software. Interactive control of optical and semiconductor properties allows the user to observe the resulting simulated TRPL transients and observe where carriers move over time.

Subtask 2.4 Extract SRV and lifetime from 2P-TRPL measurements

In this subtask we performed 2P-TRPL measurements on the single crystal CdTe sample previously described and used the model from subtask 2.3 to extract bulk lifetime and SRV from the data. We added a laser-pulse picker that allows us to measure much longer transients than before. Shown in Fig T2.4 are the 2P-TRPL transients of the CdTe sample excited at the surface and in the bulk (nominal focal depth of 5 μm below the surface). Note the time-scale of $>100\text{ns}$, allowing us to observe the long transients in the bulk of this sample. Overlaid in this figure are the predictions of our model using the extracted bulk lifetime and SRV described in this section.

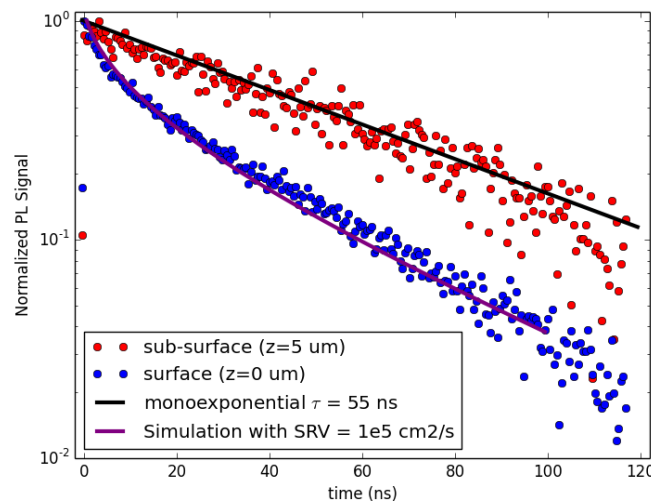


Figure T2.4. Two-photon TRPL transients of the annealed CdTe sample using the pulse picker (allowing $>100\text{ ns}$ transients to be measured).

Recap of specific tasks:

We have developed and implemented a model that can simulate the full optical and electronic processes in the TRPL experiment and fit experimental data for extracting the bulk recombination coefficient and surface recombination velocity. We have used our model to extract a bulk minority carrier lifetime of 55 ns and a surface recombination velocity of 1.0×10^5 cm/s from an annealed CdTe single crystal sample.

Task 3: Three Dimensional Lifetime Tomography

The key goals of this task was to demonstrate true 3D tomography capability. There are two phases within this task: (1) Subtask 3.1 where we integrated 3D scanning capability and determined the lateral resolution of the system and (2) Subtask 3.2 where we created 3D maps of lifetime in CdSe materials.

Subtask 3.1.1 Integration of 3D scanning

In order to successfully demonstrate 3D 2P-TRPL we have created a modular hardware/software system that allows for 3D confocal scanning and acquisition of multiple data streams, including lifetime data and spectral information. A diagram of the system components is shown in Fig T3.1. The successful completion of this task has led to 3D scans of CdTe materials described in Sub-Task 3.2.

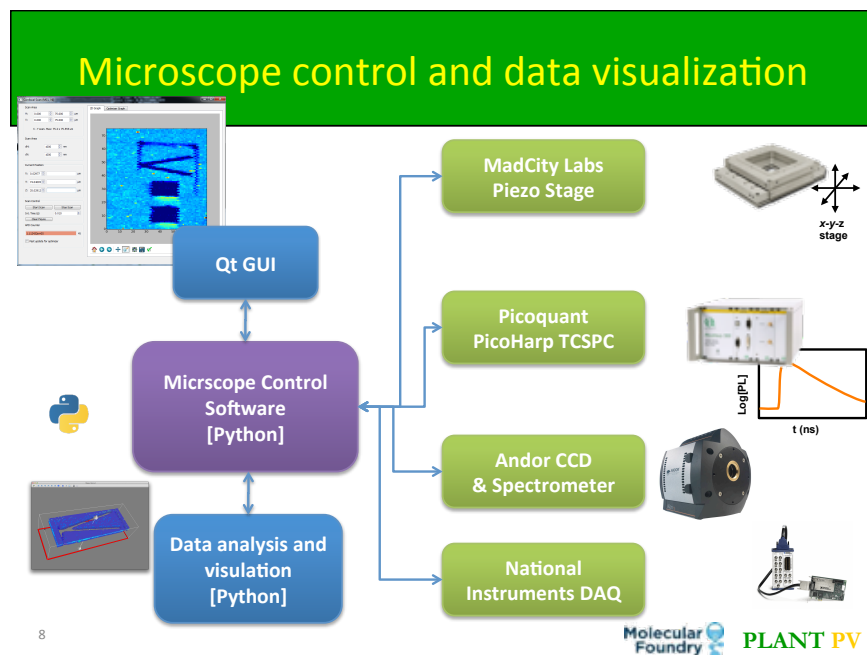


Figure T3.1. Diagram of system components for the 3D 2P-TRPL microscope.

Subtasks 3.1.2 and 3.1.3 Lateral resolution measurements

With the added capability of 3D scanning, we needed to validate the lateral scanning resolution of the system. To do this we modified our previous depth resolution test sample by focused-ion beam nano-patterning. This sample is a double InGaN/GaN/InGaN quantum well (QW) stack on a sapphire substrate grown using MOCVD as described previously in our report for Task 1. This sample was subsequently patterned with test patterns by Shaul Aloni using a focused-ion beam (FIB) tool. The FIB removed the emissive QW layer in certain regions, thus allowing for lateral contrast between patterned and unpatterned regions as shown schematically in Fig T3.2b. Figure T3.2a shows a lateral 2P-PL scan of the resolution wedge test pattern. Dark blue regions are areas where the FIB has removed the emissive QW layer. The resolution is determined by the narrowest point where the two sides of the wedge can be distinguished. Figure T3.2c shows the lateral / depth (y-z) cross-sectional map of PL from this sample. Here the small bright area in the middle is the narrow luminescent part of the wedge. The lateral resolution is measured by fitting a Gaussian to the width of this narrow region. We find that the FWHM of this emission is 600 nm, which is the current lateral resolution of our microscope.

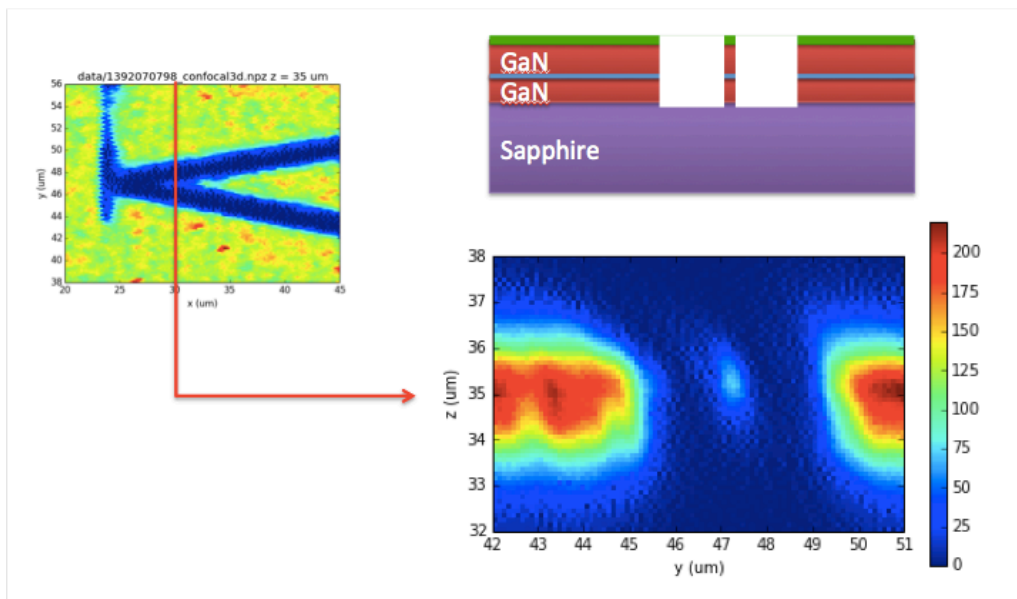


Figure T3.2. Lateral resolution test. (a, left) Lateral 2P-PL scan of the wedge-patterned QW sample. Dark blue regions are areas where the FIB has removed the emissive QW layer. (b, top) Depth cross-section schematic of the FIB cut into the QW sample. (c, bottom) Depth cross-section 2P-PL map measured at the narrow end of the wedge.

Subtask 3.2: 3D 2P-TRPL of CdSe

As a first demonstration of the 3D tomography capabilities of our technique, we have investigated sub-surface grain boundaries in poly-crystalline CdSe. This sample is from a boule of multocrystalline-CdSe grown by the Brian Riley at PNNL. We scanned the full range of motion of our scan stage (75x75 μm laterally, 50 μm in depth). At each point we collect a lifetime decay trace and fit the initial decay to ascribe a lifetime to each location. Figure T3.3a shows the slice of this 3D dataset at the surface of the sample. We note reduced PL intensity at scratches induced by the polishing process of this sample. Coincident with the reduced PL intensity, we also note reduced lifetime indicating surface defects induced by the scratches. Figure T3.3b now shows a cross-sectional depth cut from the 3D data set. Near the surface of the sample we see the cross-sections of the scratches observed in the x-y slice in Fig T3.3a. We note a contrast between surface and sub-surface lifetime with the lifetime near the surface generally being lower when compared to the bulk. In addition to this general trend, we note additional inhomogeneities in the lifetime map below the surface. Most notable is the diagonal line of reduced lifetime, which we ascribe to a grain-boundary. This sub-surface grain-boundary can be seen in even more striking detail in a 3D iso-surface rendering of this data shown in Figure T3.3c. From this 3D data it is clear that this grain-boundary extends across the scanned volume and deeper into the sample.

Three-dimensional minority carrier lifetime mapping of thin film semiconductors for solar cell applications

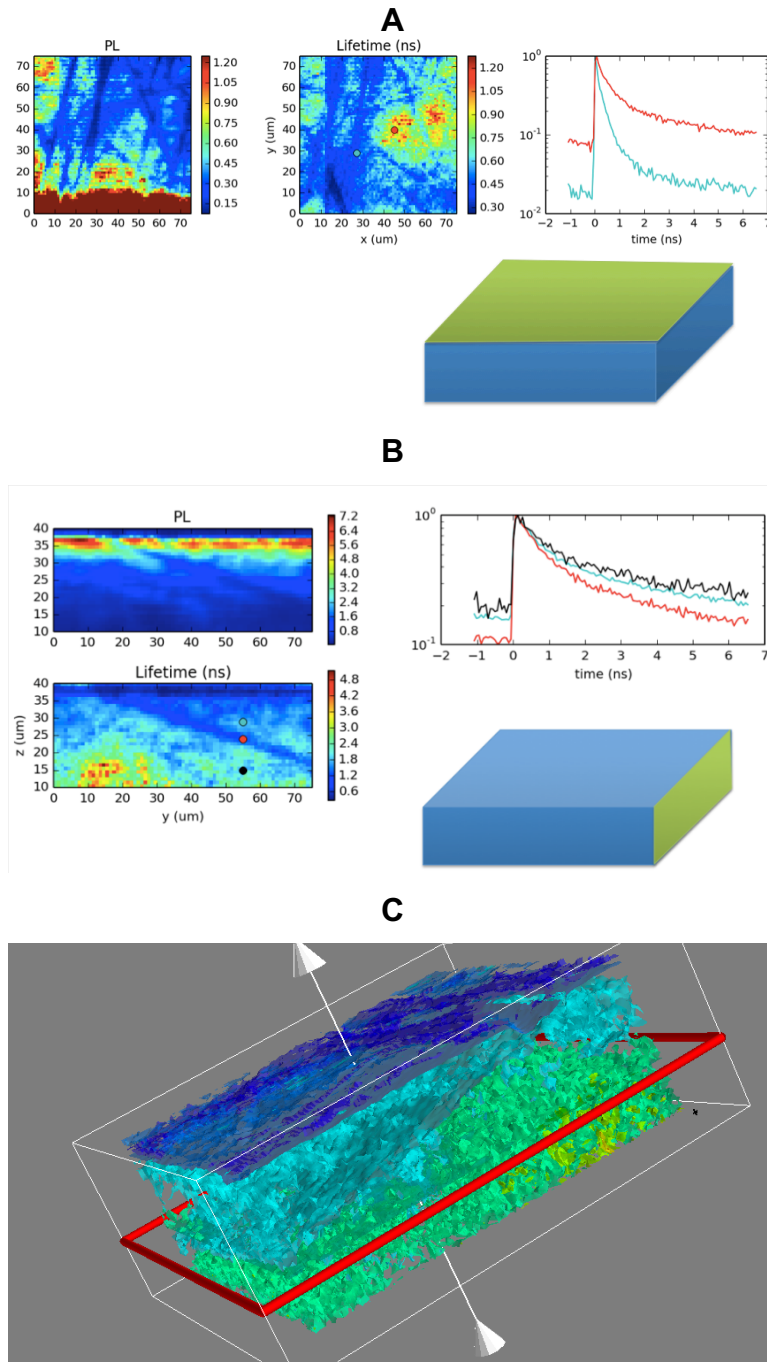


Figure T3.3. 3D tomographic lifetime scan of a poly-crystalline CdSe sample. (a) Lateral surface slice of the data. Surface scratches due to polishing are visible. (b) Depth cross-section slice of the data. A grain boundary is visible as a reduced lifetime line diagonal across the cross-section. (c) 3D map of lifetime. The grain boundary is visible as a reduced lifetime iso-surface that cuts across the scanned diagonally region.

Additional 3D measurements on CdTe poly-crystalline materials

As a second test of the 3D tomography capability of the 2P-TRPL microscopy system we performed measurements on a multicrystalline CdTe sample provided by PNNL.

The lifetime traces in this dataset exhibited non-monoexponential decay and thus biexponential fits were used to quantify carrier lifetime in the sample. Figure T3.4a shows depth cross-section maps of total PL intensity (left), short lifetime component from the fit (τ_0 , center) and long lifetime component (τ_1 , right). Representative lifetime traces are shown in Fig T3.4b. We note again that the surface has much shorter lifetime than the sub-surface. There is also significant inhomogeneity in the sub-surface lifetime at multiple length scales: large grain-like regions with different lifetimes as well as small point-defect-like regions of reduced lifetime. Figure T3.4c shows 3D iso-surface projections of the full 3D tomographic lifetime map. The short lifetime component is shown on the left and the long component is on the right.

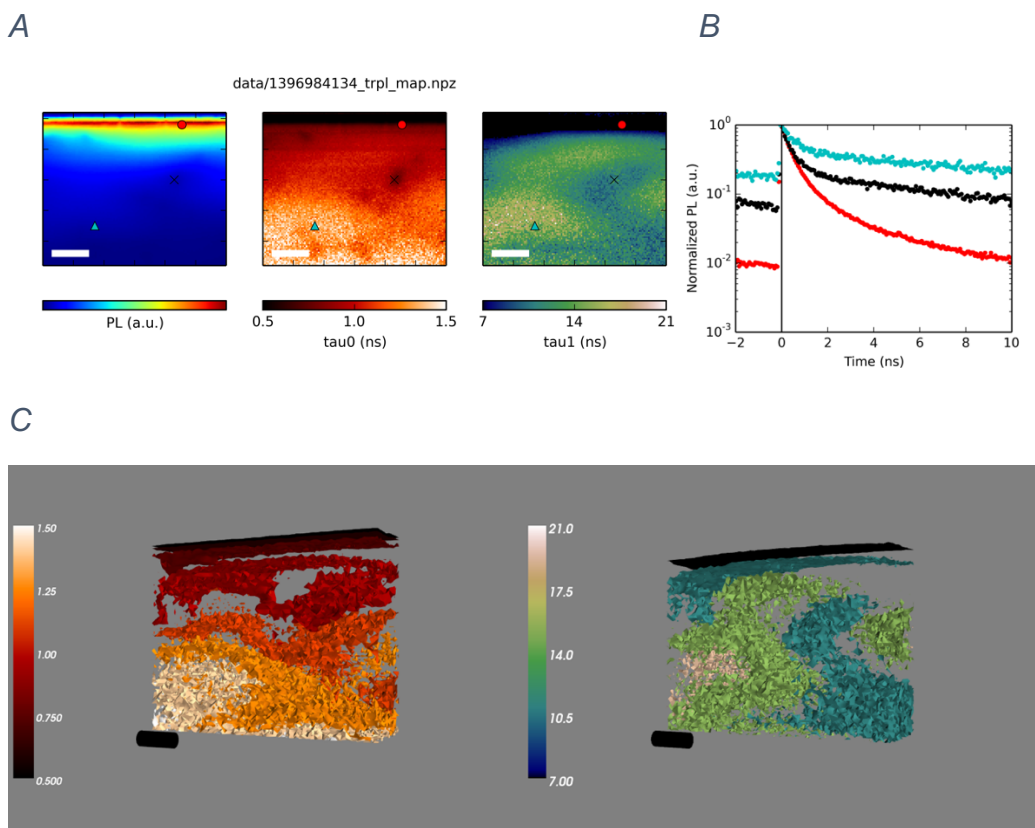


Figure T3.4. 3D tomographic lifetime map of a poly-crystalline CdTe sample. Biexponential fits are performed at each point in the 3D volume. (a) 2D depth cross-sections of the 3D data. (b) Representative lifetime traces. (c) 3D iso-surface plot of biexponential fit lifetimes of 3D data set. Scale bars are 5 μm .

Task 4 Two-photon laser-beam induced current (2PIC)

In Task 4 we developed and implemented the two-photon induced current technique (2PIC). With this technique we were able measure completed solar cells to study the charge collection efficiency inside the thin films of conventional CIGS.

Subtask 4.1: 2PIC capability build out

In order to measure photocurrent in the two-photon microscope, we have added additional electronics and integrated them into the microscopy control software. In order to perform low-noise photocurrent measurements we have implemented a lock-in technique to isolate photocurrent generated solely from the focused laser excitation. This scheme is schematically shown in Fig T4.1.

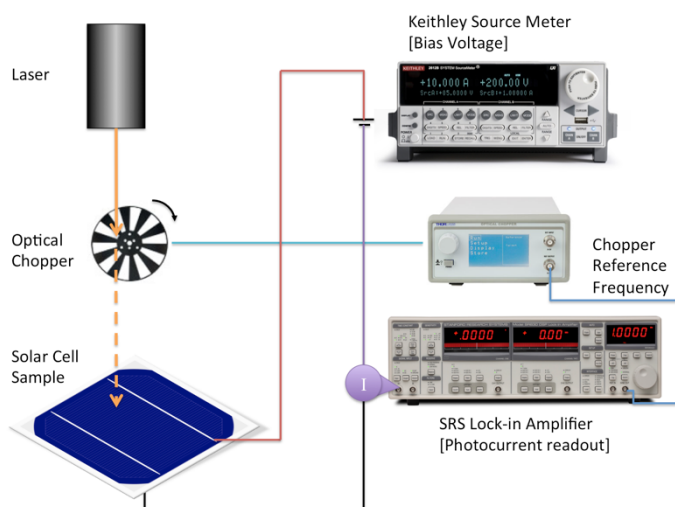


Figure T4.1 Schematic diagram of two-photon induced current (2PIC) system. A lock-in amplifier collects photocurrent generated by a focused laser. The laser's two-photon excitation spot is moved in three-dimensions in the sample while photocurrent is recorded.

Subtask 4.2 Depth-of-Focus 2PIC on CZTS solar cells

We have obtained high-efficiency CZTSSe solar cells from the Mitzi group at IBM and Duke University and performed two-photon photocurrent tomography on the device. The device was previously characterized by our collaborator to show 10.5% efficiency as shown in performance data in Fig T4.2. We have been able to connect this device to our microscope using the photocurrent electronics described in Fig T4.1. Given the narrow bandgap of 1.1eV of the sample, we excited the sample with our laser tuned to 1300 nm, to allow for two-photon absorption and minimal linear (1-photon) absorption. The power dependence of measured laser-induced photocurrent shown in Fig T4.3 confirms that we are able to achieve two-photon excitation. At higher powers we see that photocurrent is proportional to nearly input power squared, indicating that two-photon processes are occurring.

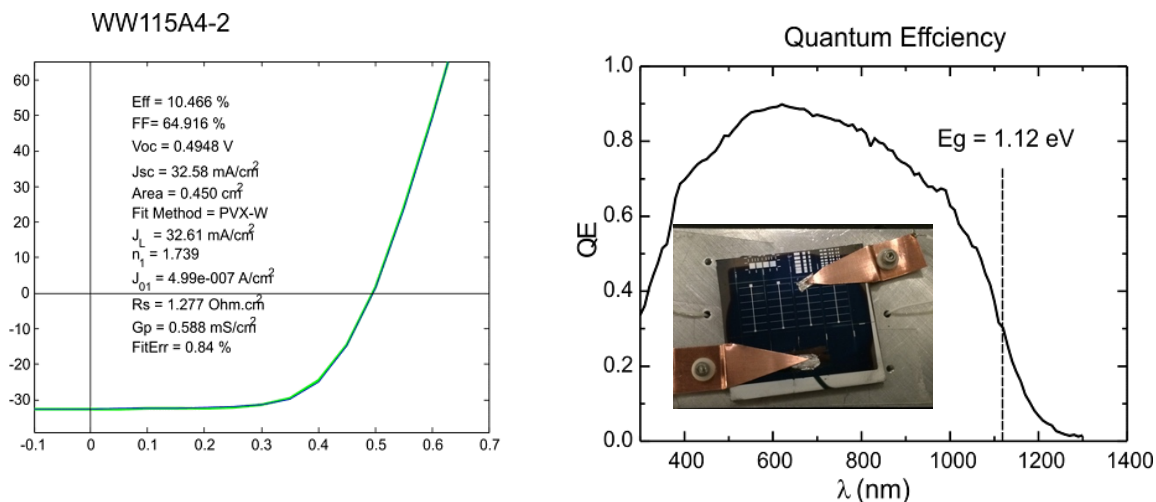


Figure T4.2. CZTSSe device performance data from Mitzi group along with a photograph of the sample used for 3D photocurrent measurements.

This sample has grains of 1 to 2 μm in size. We are able to visually inspect the surface roughness caused by these grains using wide-field optical microscopy, as demonstrated by the optical micrograph in Fig T4.4a. Next we are able to perform two-dimensional 2P photocurrent maps of the same region of the sample. The resulting photocurrent map is plotted in Fig T4.4b and as a contour overlay on Fig T4.4a.

It is clear that there is significant photocurrent variation across the sample, with contrast seen at the length-scale of the film grains (1-2 μm). Surprisingly, we find that the laser-induced photocurrent varies by a factor of two on these length-scales, suggesting strong inhomogeneity in device performance on a grain-to-grain basis.

In addition to two-dimensional photocurrent mapping, we are able to perform 3D tomographic maps of 2P laser-induced photocurrent. In Fig T4.5 we show a 3D photocurrent scan of 30x30 μm area of the film. The lateral inhomogeneity is visible through out the volume. In the depth direction we observe enhanced photocurrent when the laser focus impinges on the active layer, however due to the small thickness of the film, we do not clearly resolve a change in photocurrent within the layer.

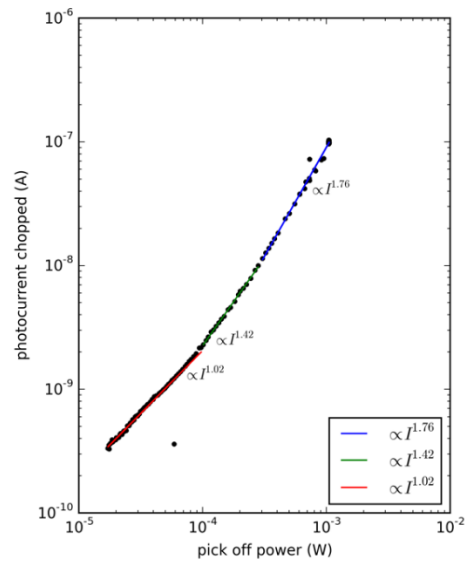


Figure T4.3. Power dependence of 2P laser-induced photocurrent (2PIC) on CZTSSe solar cell. At higher excitation powers we are in the two-photon excitation regime.

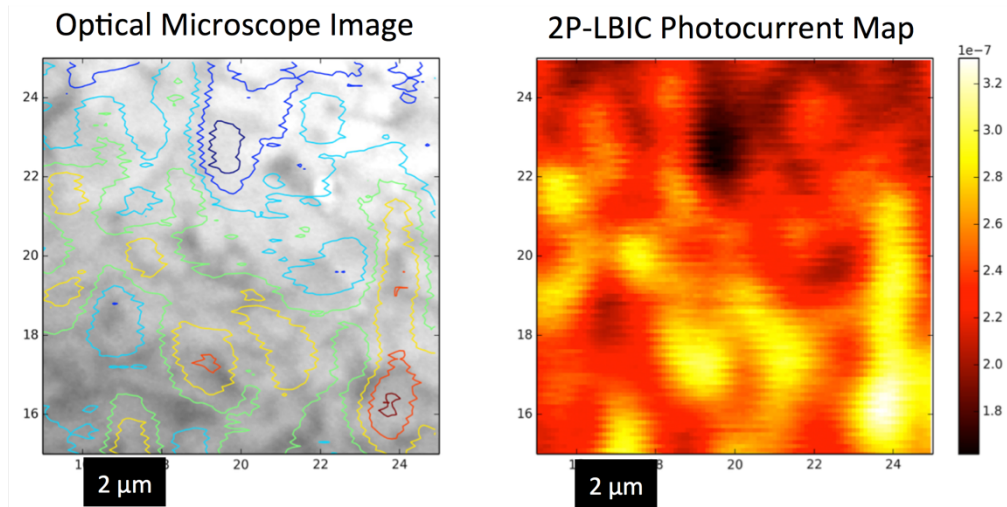


Figure T4.4. (a) Optical Micrograph of the surface of the CZTSSe solar cell. (b) Two-photon laser-beam induced current map of the same region as (a), color-scale units are photocurrent Amps.

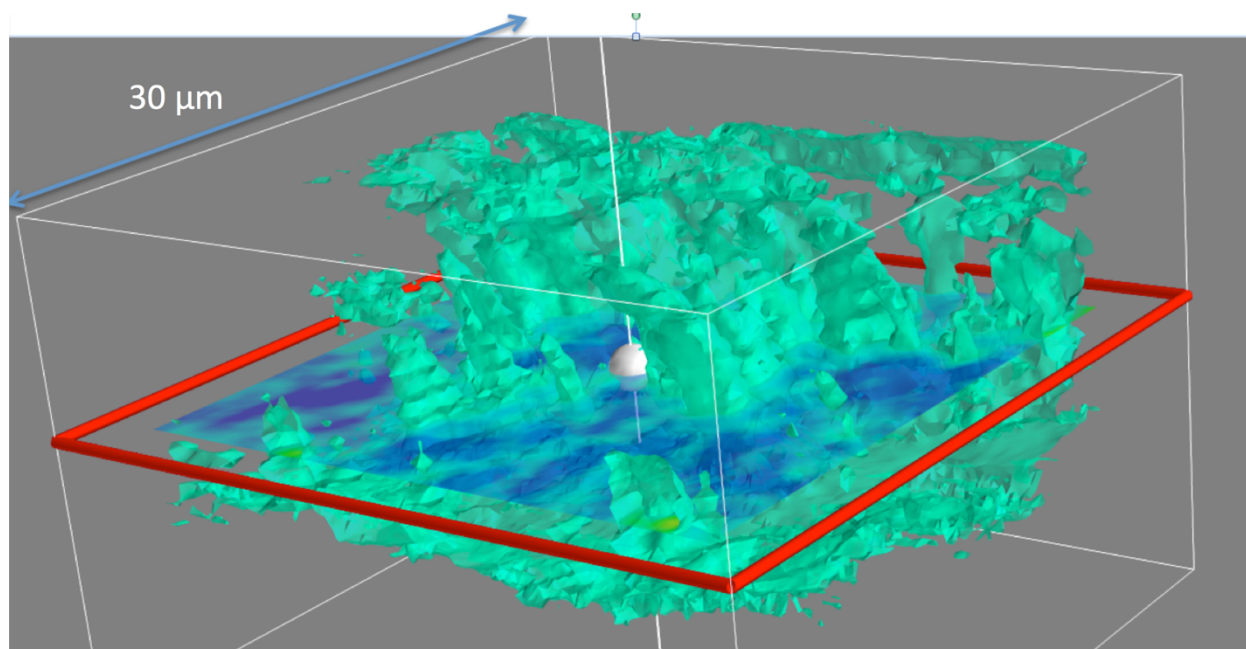


Figure T4.5. 3D photocurrent map of a 30x30µm region of the sample with a 20µm depth scan.

Task 5. Two Photon characterization and defect analysis of CdTe PV

The 2P-TRPL method developed in the previous tasks is now applied to a specific industrially-relevant material system in Task 5. In this task we have used the high-resolution 3D probing of carrier lifetime to characterize the optoelectronic behavior of buried grain boundaries and other defects in CdTe films. We have developed two different collaborations on this material system, and are currently preparing a manuscript for a peer-reviewed submission.

2P-TRPL analysis of isolated grain boundaries in CdTe bi-crystals

We have collaborated with Robert Klie at UI Chicago and their BRIDGE team to measure lifetimes near carefully isolated grain boundaries in manufactured bi-crystals. By working with these well-controlled samples we hope to measure the recombination dynamics at specific grain boundary angles and extract information about carrier diffusion length. Figure T5.1 shows initial two-photon lifetime results taken on a bi-crystal of CdTe with a 111-face 5-degree boundary. A surface lifetime scan (Fig T5.1c) shows that surface has polish scratches that reduce lifetime obscuring the lifetime change near the grain boundary. However, if we push the 2P excitation deeper into the sample we are measure lifetime (Fig T5.1d) that is unaffected by the surface of the

sample. Here we clearly see a strong reduction in lifetime along the entire length of the grain boundary and a uniform longer lifetime away from the boundary. The contrast between Fig T5.1c (surface) and Fig T5.1d (bulk) clearly shows how surface defects can typically make extracting lifetime information difficult, and how 2P microscopy can allow us to measure lifetimes without the surface effects dominating the measurement.

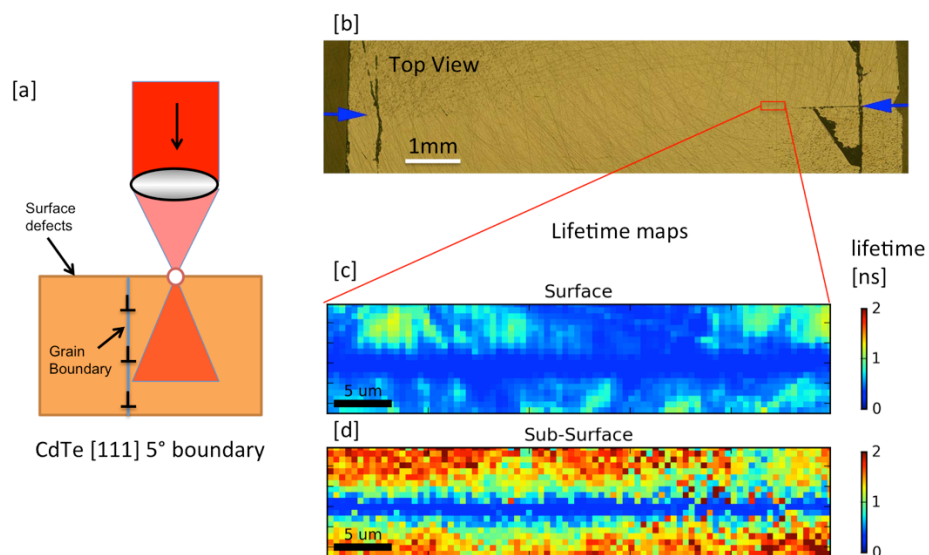


Figure T5.1. Two-photon measurements of bi-crystal CdTe from Robert Klie, UI Chicago. (a) Schematic of bi-crystal measurement. (b) Optical micrograph of the bi-crystal. The two crystals are on the top and bottom of the image and the grain boundary interface between crystals is indicated by the blue arrows. (c) Near-surface and (d) sub-surface two-photon lifetime maps of bi-crystal near grain-boundary.

To measure the effect of the grain boundary on recombination we performed two-photon depth cross-sections shown in Fig T5.2. In Fig T5.2a we show a lifetime depth cross-section map near the grain boundary. The grain boundary cuts vertically through the map and shows reduced lifetime along the boundary. We also see that the top surface has reduced lifetime due to polishing defects also seen in Fig T5.1. What is most useful from this dataset is the change in the subsurface lifetime as we approach the grain boundary shown as a line cut in Fig T5.1b. In this plot of lifetime vs distance from boundary we can see the spatial extent of the effect of grain boundary recombination due to diffusion of carriers to the grain boundary. We believe that this data will allow us to extract both grain boundary recombination velocity and bulk carrier diffusion lengths for this material system.

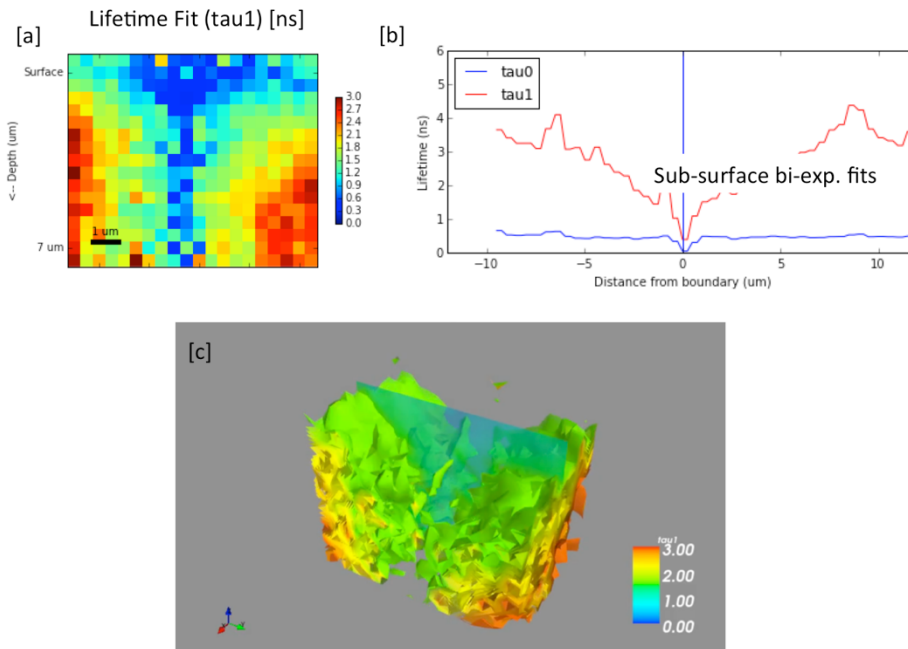


Figure T5.2. Depth cross-section Two-photon lifetime scan. (a) Lifetime map (b) Sub-surface lifetime vs distance from grain-boundary. (c) 3D lifetime map of the grain-boundary

Initial CdTe poly-crystal thin film 2P-TRPL measurements

We have also been working with collaborators at NREL (Wyatt Metzger et al.) that have provided us with poly-crystalline CdTe thin films with grain sizes around 5-10 μ m. These films have various processing conditions allowing us to see the effect of treatments on local carrier lifetime at the surface and bulk of the film. Additionally, these samples allow us to measure inter-grain and intra-grain variation in lifetime using our 2P-TRPL technique. Figure T5.3 shows some of our early results on one such sample. Here we see a 2P-TRPL depth cross-section where two pyramidal grains are visible, a grain boundary separates the two vertically through the scan. Fig T5.3a and T5.3b show the biexponential fit components of lifetime throughout the cross-section. We note generally a reduced lifetime near the surface of the pyramids attributed to surface recombination. There is clearly a region of significantly reduced lifetime at the interface between the two grains, indicating the grain boundary has adversely effected carrier lifetime in and nearby the boundary. Fig 3c shows the PL intensity drop off below the surface due to reabsorption. This reabsorption trend is borne out in Fig T5.3c where we see a red-shift in PL emission spectrum with increasing depth into the film. In addition to this general trend in PL intensity, the PL intensity is also lower at the grain boundary between the two pyramidal grains, also showing a strong effect of grain boundary on radiative recombination.

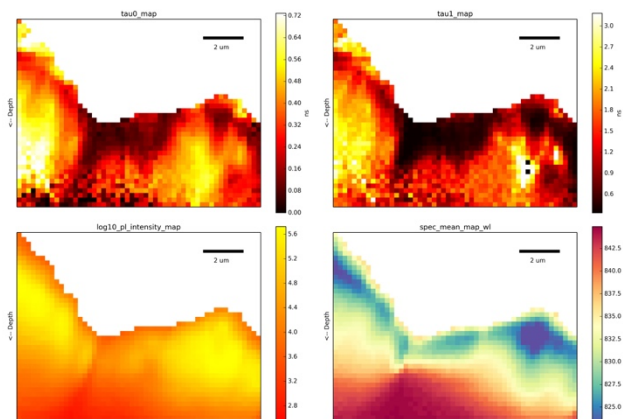


Figure T5.3. Depth resolved 2P-TRPL lifetime of a grains of a CdTe film. Pyramidal grains are observed, along with reduced lifetime regions between the grains (at grain boundaries).

Lifetime at Grain Boundaries in CdTe polycrystalline films

To better probe the effect of grain boundaries throughout the CdTe film, we worked with NREL to produce optically flat samples using mechanical polishing. This allowed us to observe sub-surface grain boundaries and buried interfaces without scattering due to the as-grown rough surface. With these samples we have been able to perform large area 3D lifetime scans over many grains as shown in Figures T5.4. We generally observe strong non-radiative recombination at grain boundaries that causes a sharp drop in PL intensity and PL lifetime at and near the grain boundaries. We also observe longer, more uniform lifetime in the centers of the grains where carriers do not recombine as fast. By performing 3D maps shown in Figure T5.4c we also observe a both reduction in lifetime and change in grain morphology as we approach the buried interface in these samples.

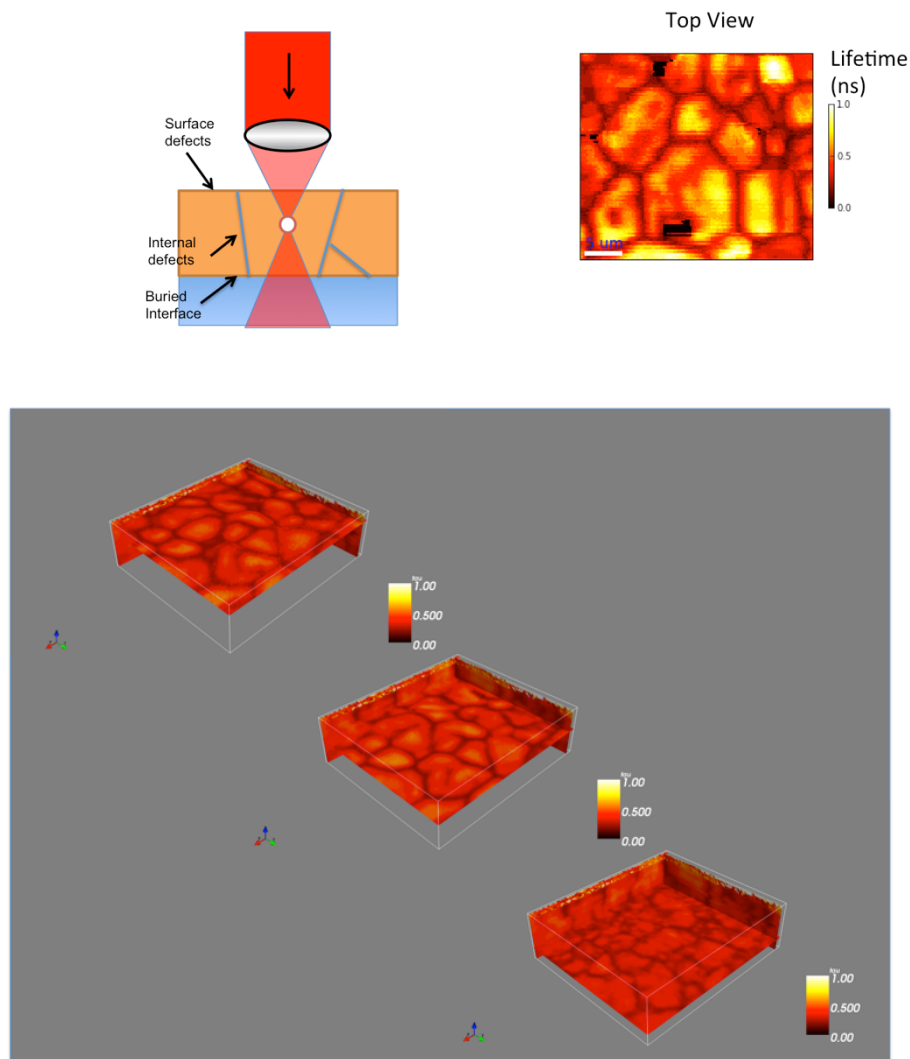


Figure T5.4. (a) Schematic of two-photon microscopy measurements on polycrystalline CdTe films. (b) Lateral two-photon lifetime map of a surface polished polycrystalline CdTe Film. Grain boundaries show significantly reduced lifetime compared with the grains. (c) 3D scan of polycrystalline CdTe film from Wyatt Metzger (NREL). Three slices of scan volume show surface, bulk, and buried interface maps of carrier lifetime in the sample.

Effects of CdCl₂ processing on grain boundaries in CdTe polycrystalline films

Once we found that this type of 3D mapping yielded interesting information about grain boundaries, we used the technique to try to answer a very scientifically relevant question about CdTe: How does the typical CdCl₂ treatment change the local carrier dynamics in a polycrystalline solar cell? This treatment has been used for decades to take low performing cells and bring them up to efficiencies that now rival crystalline

silicon cells. Despite this long history of use and study, it is not completely understood what mechanisms cause the CdCl_2 treatment to improve performance. Specifically, it is not clear how CdCl_2 affects carrier recombination at grain boundaries. We have performed 3D 2P-TRPL measurements on NREL-grown polycrystalline CdTe films, pre- and post- CdCl_2 treatment, analyzed the lifetime information, and have prepared a manuscript for submission on this work.

Figure T5.5 shows representative slices of the 3D maps of carrier lifetime for the two samples: on the left an as-deposited CdTe poly-crystal film and on the right a similar CdTe film post treated with CdCl_2 . Figures T5.5a and T5.5b show lateral (x - y) slices of the 3D data set at representative depth in the sample: (1) polished top surface of the CdTe layer (2) the bulk of the CdTe layer ($5\mu\text{m}$ below the surface) and (3) The CdTe/CdS interface.

The first thing that jumps out from these maps is the dark lines in the shape of grain boundaries on the as-deposited map (left) where local carrier lifetime is reduced significantly compared with neighboring areas. EBSD measurements (see Fig 3) show that these lines of reduced lifetime do indeed correspond to CdTe grain boundaries and thus demonstrate that carrier recombination is happening more rapidly near the grain boundaries than in the grain interiors. Unlike the as-deposited sample, the CdCl treated sample (right) shows a more homogeneous distribution of local carrier lifetime without characteristic reductions at grain boundaries.

The visibility of grain boundaries in the as-deposited sample (and the lack of visible boundaries in the CdCl_2 treated sample) are more than surface deep. Figure T5.5c and T5.5d show depth cross-sections of the respective samples. We see on the as-deposited cross-section lines of reduced lifetime that extend from the top of the film to the bottom, revealing grain boundary recombination throughout the film. We note that we also see a change number of grains from top to bottom, illustrating grain coalescence during growth: columnar grains are seen in the top $5\mu\text{m}$ of the film, while smaller seed grains are observed near the CdTe/CdS interface.

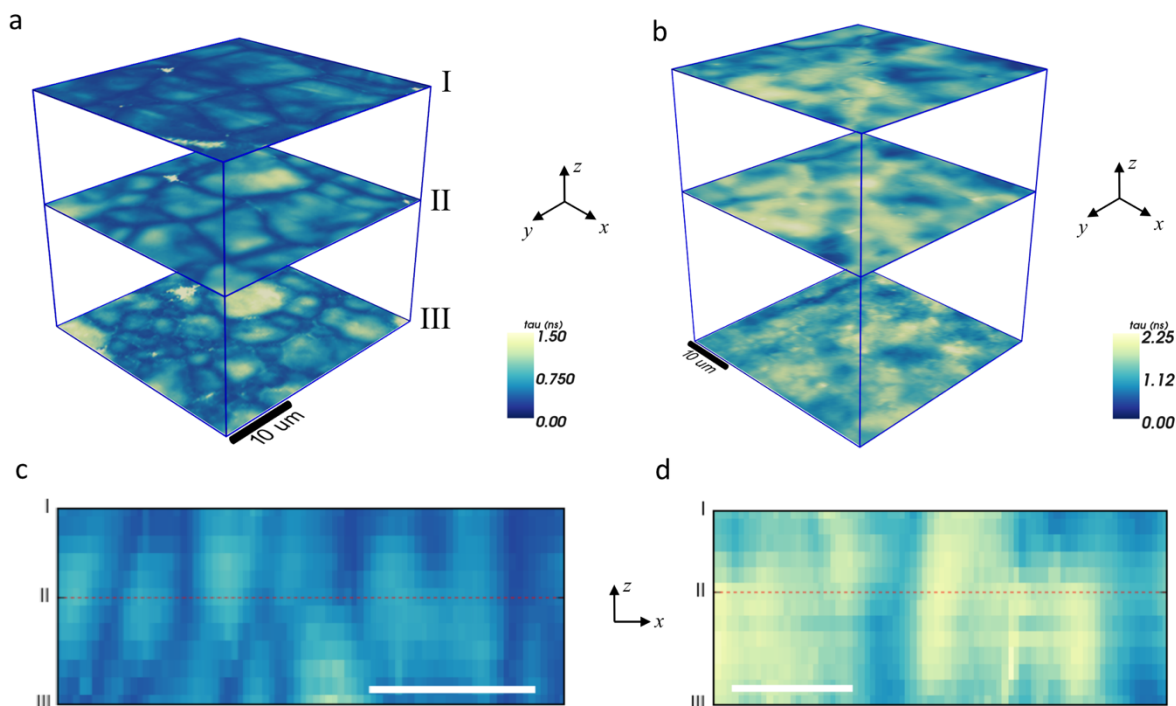


Figure T5.5. 3D tomographic comparison of carrier lifetimes between as-grown and CdCl₂-treated CdTe films. (a,b) Horizontal cuts (i.e., planes parallel to the top surface) of the carrier lifetimes at discrete sample depths (I: surface, II: bulk, III: buried CdTe/CdS interface) for a) the as-deposited sample and (b) the CdCl₂ treated sample. (c,d) Representative depth cross-sections (i.e., orthogonal to the top surface) of carrier lifetimes for the (a) as-deposited and (c) CdCl₂-treated samples. Scale bars are 10 μm.

We have qualitatively described that we see contrast between the as-deposited and CdCl₂-treated samples in regards to grains vs grain boundary lifetime contrast, but if we wish to quantify this contrast we must categorize the voxels of data. Electron Back-Scatter Diffraction mapping allows us to measure local crystallographic orientation at the surface of the sample. From this information we can independently map grain locations (areas of continuous local crystallinity) and grain boundaries. The right insets in Fig T5.6a and T5.6b show EBSD maps of the as-deposited and CdCl₂ treated samples, respectively. The regions of EBSD and 2P-TRPL maps are correlated using fiduciary markers. For the case of the as-deposited sample lines of reduced lifetime are clearly correlated with EBSD grain boundaries. For the CdCl₂-treated sample we show the EBSD grain boundary overlay in red in Fig T5.6b. In this case, no reduction in lifetime along these boundaries is seen, in fact some of the boundary areas appear to have longer lifetime than neighboring grains.

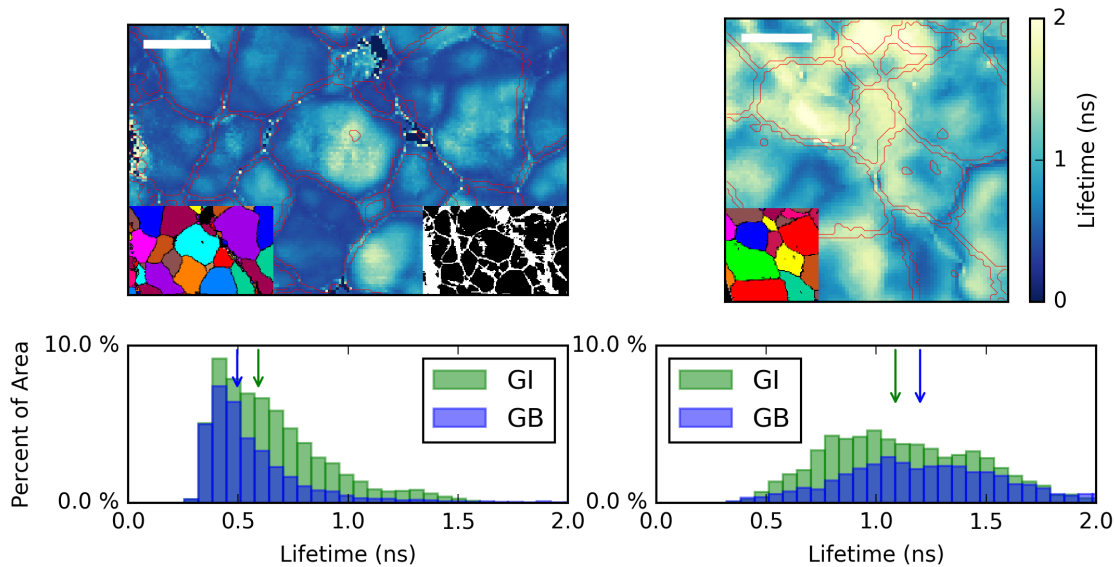


Figure T5.6. Carrier lifetimes in grains and at grain boundaries in as-deposited and CdCl₂-treated CdTe films. (a,b) Correlation between EBSD grain mapping with 2P-TRPL maps near surface of the samples. Scale bars are 10µm. Insets are reduced in size by 3x. (a) Carrier lifetime map of the as-deposited sample overlaid with red contours that mark grain boundary regions. (b) Similar map of carrier lifetimes in the CdCl₂-treated sample. (a,b) Left insets show the corresponding EBSD maps of the regions, showing the locations of grains and grain-boundaries. Overlaid red contours show the co-aligned grain boundaries from the EBSD micrographs. (a) Right inset shows a slice of PL-intensity threshold map used in full-volume GI/GB separation. (c,d) Histograms of GI (green) and GB (blue) lifetimes in this near-surface layer for the two samples. Arrows note the median lifetime value for each voxel type (green for GI, blue for GB). (c) As-deposited sample. (d) CdCl₂-treated sample.

EBSD is sensitive to the surface and allows us to correlate grain structure to surface lifetime maps. For the as-deposited sample we can take this further, by segmenting the data throughout the thickness of the film. In this sample the EBSD data closely matches the location of sharp reductions in measured carrier lifetime in the 2P-TRPL map (Fig T5.6a) as well as PL intensity (not shown) near the surface. Thus for the as-deposited sample we use this sharp drop of PL intensity at grain boundaries throughout the volume as a threshold to locate grain boundaries. A corresponding slice of this threshold map is shown in the right inset of Fig T5.6a. This threshold map closely correlates with the grain boundaries revealed by EBSD.

In addition to extracting statistics on the lifetime contrast between grain interiors and grain boundaries near the surface of the material, these 3D lifetime maps allow us to explore variations in carrier lifetime throughout the depth of the film. For the case of the as-deposited sample, our classification of voxels into GI and GB based on their PL intensity, allows us to explore trends in carrier lifetime throughout the depth of the film within grains and at their boundaries. Figure T5.7a shows a representative 2P-TRPL depth cross-section of the as-deposited sample. The inset shows the separation of GI and GB voxels as determined by a PL intensity threshold. With this classification over the entire 3D volume, we show in Fig 4b the median lifetime of the grain interior (green) and grain boundary (blue) areas as a function of depth into the sample for the as-deposited sample. General trends of the entire area are: (I) median lifetime is shortest at the CdTe sample surface, which is where the back contact of the cell would be placed; (II) the lifetime increases towards the bulk, peaking at approximately $5\mu\text{m}$ beneath the top surface; and (III) the lifetime then decreases near the CdTe/CdS junction where the CdTe growth is initiated. These trends apply to both GI and GB areas, but are more pronounced in the GIs. As summarized in Table 1, the grain interior lifetimes increase from 0.37 ns at the CdTe surface to 0.70 ns in the bulk, and then decrease to 0.66 ns at the CdTe/CdS interface. The GB lifetimes are uniformly smaller than the GI lifetimes throughout the depth of the film, and increase from 0.28 ns at the CdTe surface to 0.43 ns in the bulk and falling slightly to 0.40 ns at the CdTe/CdS interface.

Enhanced carrier relaxation rates are commonly associated with increased non-radiative relaxation pathways that are mediated by defects. At the exposed top surface short carrier lifetimes are typical of CdTe films (and other semiconductors) and arise mostly from surface-related material defects induced by such things as intrinsic surface states, atmospheric exposure, and mechanical processing such as polishing. We note that, lifetime measurements on unpolished samples also exhibit reduced lifetime compared to sub-surface areas, thus demonstrating that a polishing treatment is not the sole source for increased surface recombination. By using multi-photon excitation to confine the excitation volume well into the bulk, the interference from such surface-related processes is minimized and the measured properties better reflect the intrinsic bulk properties. The reduction of carrier lifetimes at the buried interface likely result in a combination of interface-related defects and grain-boundary-induced recombination. Throughout the film, grain boundaries have substantially reduced lifetime compared with grain interiors. The buried junction is the site of initial CdTe growth on CdS, and therefore there are smaller and more numerous seed grains that coalesce as the film grows. This leads to a higher density of grain boundary recombination near the CdTe/CdS interface. Since charge separation occurs at this interface, recombination near the junction is a critical hindrance to device performance in CdTe solar cells².

Similar depth analysis can be performed on the CdCl₂-treated sample as shown the depth cross-section in Fig T5.7c. Because the treatment diminishes the contrast between GB and GI regions, classification of voxels is not possible over the full volume of the treated CdTe and limited to only top surface using the EBSD measurements as

discussed in Fig T5.6. For comparison to the untreated sample, the median *surface* lifetimes in the GIs and at GBs is represented in Fig T5.7d by green and blue arrows, respectively. We note surface GI and GB median lifetimes are very close to the median lifetime of all surface voxels.

Although discerning the changes in lifetime with probe depth for GB and GI regions is not possible for the treated sample, a general trend of the bulk is still identifiable. We thus plot in Fig T5.7d the median lifetime for all voxels as a function of depth for this CdCl₂-treated sample. Again, the lifetime is reduced at the surface and the buried interface relative to the film bulk. Relative to the as-deposited sample, the variation does not follow grain structure and lifetimes are significantly improved at all depths. Again summarized in Table T5.1, the treatment improves the surface lifetime by a factor of 2 and improves the lifetime in the bulk of the film by a factor of 1.7. Most interestingly, the treatment significantly increases lifetime at the buried CdTe/CdS interface, indicating that the CdCl₂ treatment can penetrate the entire 15 μm film and significantly improve lifetimes in the critical junction region by a factor of 2. There is no appearance of grain-boundary like structures with reduced lifetime deeper in the film, which indicates that grain boundaries appear to be passivated throughout the film.

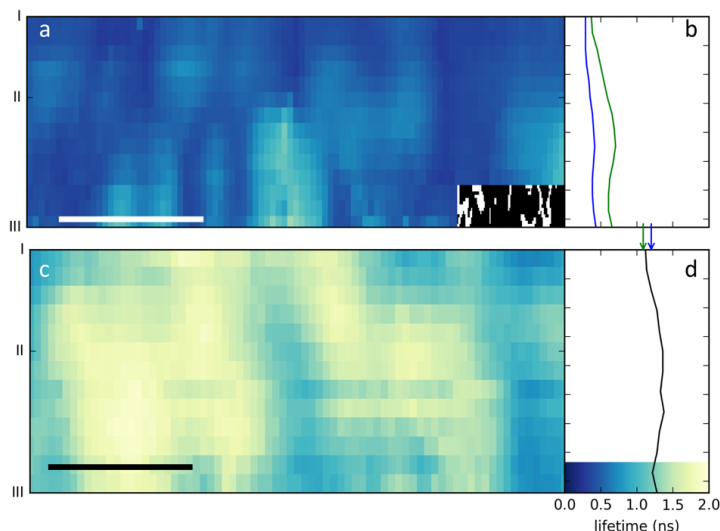


Figure T5.7 Depth analysis of carrier lifetimes in as-deposited and CdCl₂-treated CdTe films. Representative depth cross-sections of carrier lifetimes for the (a) as-deposited and (c) CdCl₂-treated samples. Scale bars are 10 μm. (a) Inset shows threshold-based separation between grains and grain boundary voxels. (b) Average carrier lifetime as a function of depth into the as-deposited sample in grain boundary regions (blue), and grain interiors (green). (d) Average carrier lifetime as a function of depth into the CdCl₂-treated sample. Blue and green arrows show average lifetime of GB and GI pixels at the surface.

	As-Deposited Sample		CdCl ₂ -treated Sample		
	Grain Interior	Grain Boundary	Grain Interior	Grain Boundary	Full Layer
I Surface	0.37 ns	0.28 ns	1.1 ns	1.2 ns	1.1 ns
II Bulk	0.70 ns	0.43 ns	—	—	1.4 ns
III Buried Interface	0.66 ns	0.40 ns	—	—	1.3 ns

Table T5.1. Summary of carrier lifetime results for both as-deposited and CdCl₂-treated sample at different depths.

We have demonstrated spatially resolved, diffraction-limited 3D carrier lifetime maps using two-photon lifetime tomography. When thin film CdTe solar cells are initially deposited, there is increased non-radiative carrier recombination at grain boundaries throughout the 3D volume of the film, and this is most pronounced in the critical junction region where small nucleation grains form at the buried CdTe/CdS interface. The data reveals that a critical function of the CdCl₂ treatment is to reduce surface, interface, and grain boundary recombination throughout the entirety of these polycrystalline films. This work indicates that removing the CdCl₂ treatment will require shifting to larger grain materials, and/or finding alternative methods to passivate the surface, interfaces, and grain boundaries.

Task 6 Microscope depth resolution improvement

This task was added during the Go/No Go process, to address the challenges we faced achieving a 1 μm depth resolution in the first half of the project. Our original goal in this task was to develop the use of solid-immersion microscopy on our two-photon microscope to push the optical depth resolution sub-micron. As described below, solid immersion did not work for our microscope and samples, likely due to optical aberrations and a lack of extreme flatness of the sample. However, we also explored two other methods of resolution improves that have yielded success. Digital post-processing techniques have allowed us to show enhanced depth resolution of conventionally-acquired data and optimized use of oil-immersion objectives have show that we can achieve 1μm nominal depth resolution.

Two-photon solid immersion microscopy

A solid immersion lens (SIL) has the capability to improve both the lateral and depth resolution of a microscopy system, but drastically increasing the possible numerical aperture of the microscope by using a high-refractive index solid lens in intimate contact

with the sample as shown in Fig T6.1a. Under ideal conditions, such a lens system can drastically improve resolution as shown in the comparison between Fig T6.1b and c. Commercially available SILs are made of silicon, for the purpose of high resolution metrology in microelectronics. Silicon, however, will not work for as a lens for most direct band-gap PV materials, including CdTe. Thus we custom sourced ZnSe hemispherical SILs for this task from Sierra Precision Optics.

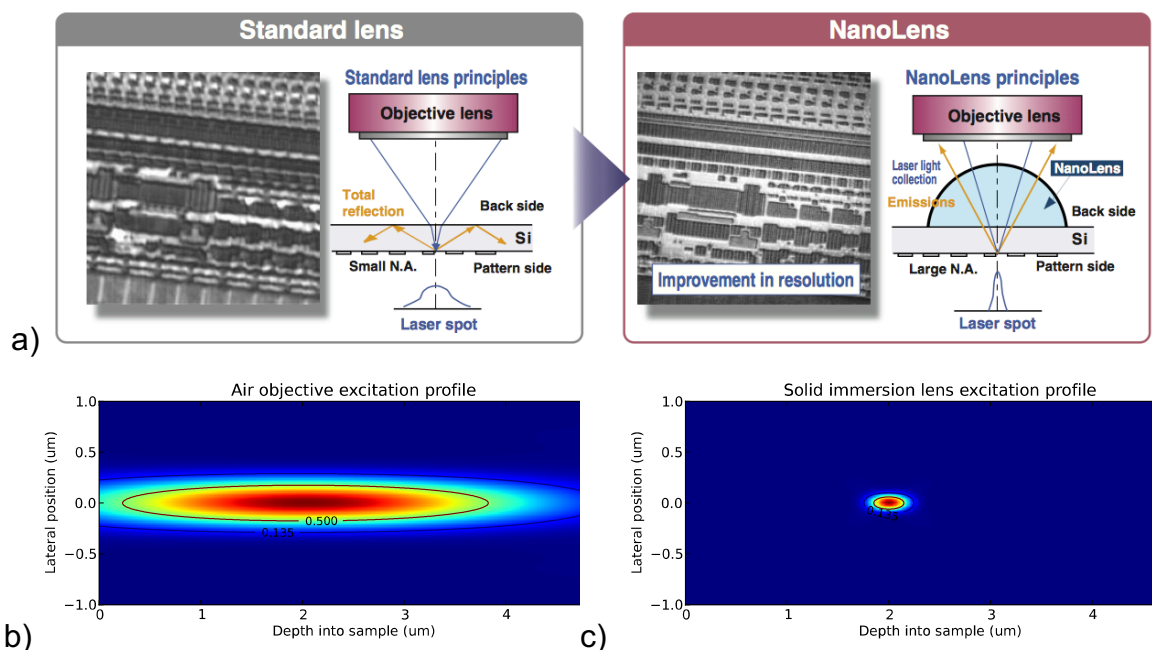


Figure T6.1. (a) Schematic of solid immersion lens for microelectronics (Figure from Hitachi). Optical simulations of the excess carrier profile for a CdTe sample ($n_1=2.9$) excited by the 2-photon mechanism at $\lambda_{ex}=900\text{nm}$ using (b) $n=0.95$ objective lens, and (c) $n=2.9*0.95$ idealized solid immersion lens.

We have performed tests these ZnSe solid immersion lenses (SIL) in with the goal of improving the depth resolution of our technique. As an initial test of our SIL incorporated tool, we tested whether or not 2P excitation through the SIL was possible. It is possible that dispersion of the laser pulse (spreading in time) in the ZnSe material could reduce the peak intensity and thus reduce 2P excitation probability. Additionally, if the optics were not correctly optimized, inadequate focusing could reduce the probability of 2P excitation. For this test we placed the SIL on a fixed custom-built holder plate and placed a small sample on the SIL as shown in Fig T6.2a. The sample was a GaInP QW sample from collaborators at CalTech with an emission band at 1.84eV (674 nm wavelength). We illuminated the sample with the laser tuned to 830 nm and analyzed the emitted light with a spectrometer. The resulting spectra with and without the SIL in place are shown in Fig T6.2b. This data illustrates that we are able to use 2P excitation through the 4mm diameter SIL with a 10x 0.3NA objective.

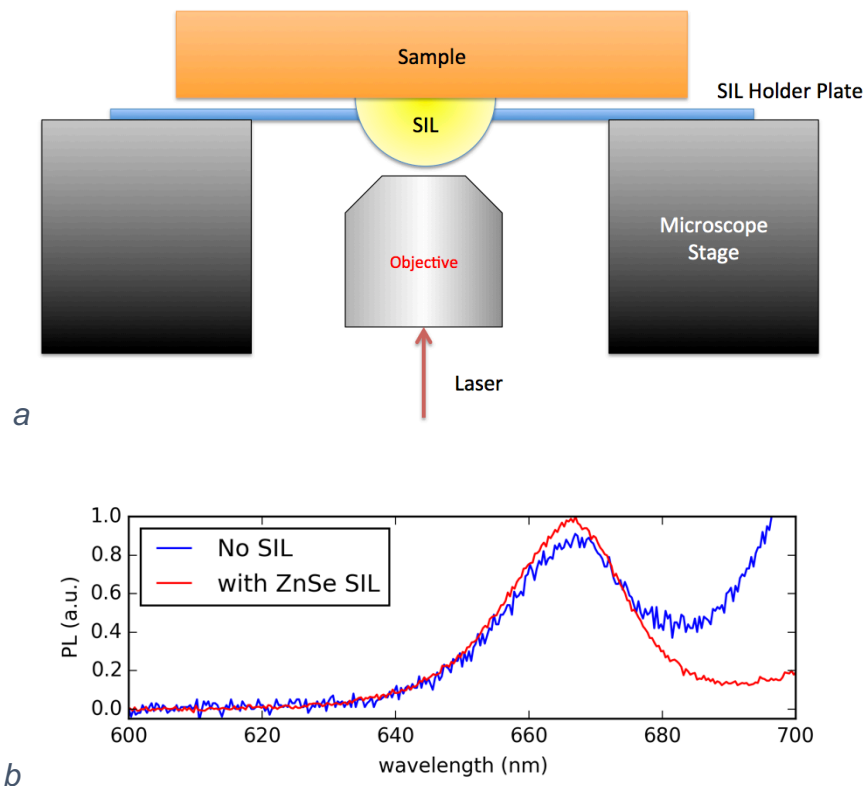


Figure T6.2. (a) Schematic diagram of solid-immersion lens test system. (b) Comparison of two-photon PL from the GaInP device with and without a SIL.

Since we showed that we could observe 2P PL emission through the solid immersion lens we then started to characterize the depth resolution of the SIL system. We have been able to use a higher numerical aperture objective (0.9NA) with appropriately long working distance to work with a 1 mm diameter ZnSe SIL. Using the same GaInP QW sample as a reference we have measured the depth resolution of the current SIL system to be $3\mu\text{m}$ as shown in Fig T6.3. In this figure we see the depth profile of the QW emission (blue) and the GaAs substrate emission (red). This depth resolution has not yet approached the theoretical sub-micron range that we had hoped, but we believe that with future appropriate aberration corrections and extremely flat samples we can approach the desired range. One possible future avenue for compensating optical aberration in the system is the use of adaptive optics. This has been shown by others to improve depth resolution in multiphoton imaging systems²¹.

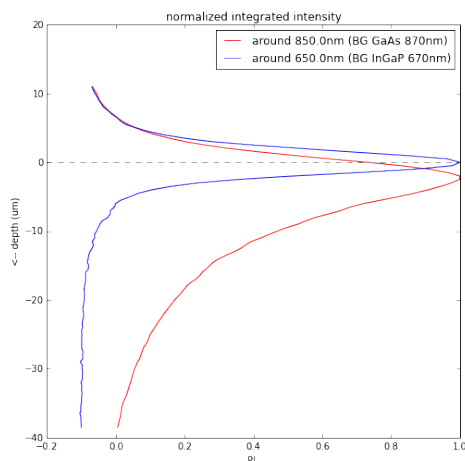


Figure T6.3. Depth profile of QW well emission imaged through ZnSe SIL and 0.9 NA objective.

Deconvolution Techniques

To complement or obviate the need for optical resolution improvement we have explored post-processing techniques to extract higher-resolution data from our current microscopy system. There are many algorithms used for image resolution enhancement in microscopy used in order to localize the origin of a signal with a precision higher than the uncertainty defined by the instrumental limits. One of the most robust and versatile ones is the Richardson-Lucy deconvolution^{22,23}. In its purest form it is an iterative procedure for recovering the latent image that is blurred by a known point spread function (PSF).

We have applied this algorithm to the data acquired from InGaN quantum well structures embedded in the GaN film. In Fig T6.4, we compare the depth profiles of the total two-photon luminescence acquired at 430 ± 15 nm and 460 ± 15 nm wavelength bands corresponding to the emission wavelength of the two QW structures. The green Gaussian is the theoretically predicted PSF of $\sim 1.7\mu\text{m}$. In the as-acquired data the positions of the two quantum wells can be only defined by measuring the distance between the maxima in the spectrally resolved emission bands. Since the light emitting structures are significantly smaller than the diffraction limited resolution, the width of these peaks can be used to estimate the PSF and is in good agreement with the calculated $1.7\mu\text{m}$ focal point size and feature within the acquired data. It is no longer the case in the digitally enhanced depth profiles. After deconvolution one can easily see that all features are significantly narrower with widths of $0.9\mu\text{m}$ and $1.2\mu\text{m}$ for the shallow and deep quantum wells structure, setting the resolving power at about $1\mu\text{m}$ and allowing localization of these features with much greater precision defined by the signal to noise ratio and spatial oversampling. In this case the features can be localized in the z-direction with sub-pixel accuracy (better than 100nm). Moreover, two maxima are clearly visible in the $460\pm 15\text{nm}$ band (the solid red curve). Since both quantum well structures emit in this wavelength range it provides another independent measure of the digitally enhanced resolution placing it below $1.2\mu\text{m}$ as well.

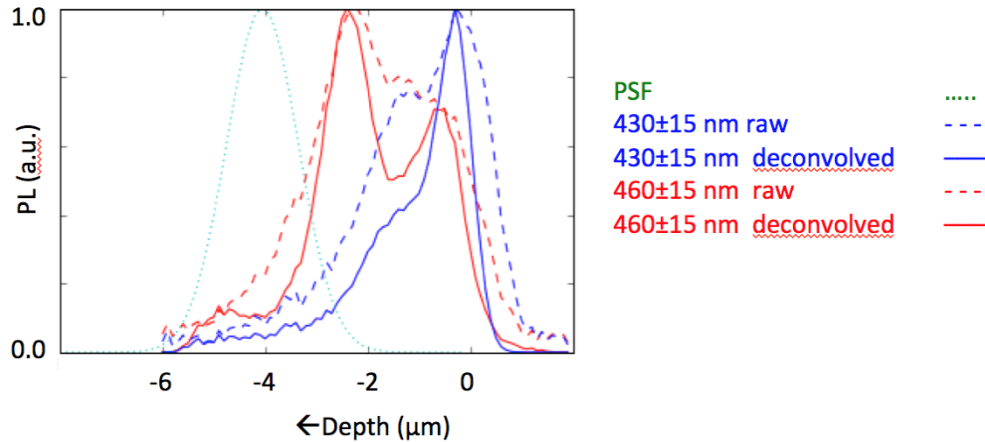


Figure T6.4. Digital resolution enhancement (deconvolution) of quantum-well data showing improved sub-micron resolving power.

Oil Immersion microscopy yields 1μm nominal depth resolution

As an alternative to using Solid Immersion lenses, we worked on using oil immersion to achieve significant depth resolution improvement. While the theoretical improvement to depth resolution is less compared to solid immersion, we have found that in practice, we are able to achieve better resolution with oil. In order to approach the theoretical maximum resolution improvement¹³, we found that we needed to completely fill the back focal plane of our oil objective, as shown in Fig T6.5. While under-filling has a slight effect of reducing lateral resolution, it has a very detrimental effect on axial (depth) resolution.

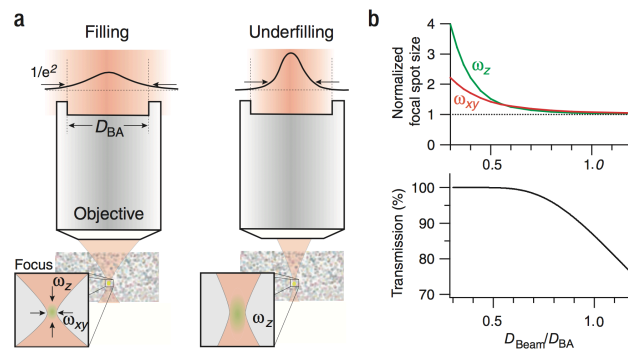


Figure T6.5. Effects of under filling or overfilling the back focal plane of a microscope objective. From Helmchen & Denk¹³.

By using a beam expander on our laser excitation path we were able to fully fill the objective and improve depth resolution to a nominal 1.0μm depth resolution as shown in

Figure T6.6. Here we use our quantum-well test sample and excite with 1100nm from our Ti:Sapphire/OPO laser system. Three photon PL yields a nominal depth resolution of 1.0 μm FWHM with a filled objective. Previous results with an under-filled objective yielded a 2.5 μm FWHM nominal depth resolution. Similarly, two photon excitation with a 550 nm laser, yields a 1.1 μm FWHM nominal depth resolution.

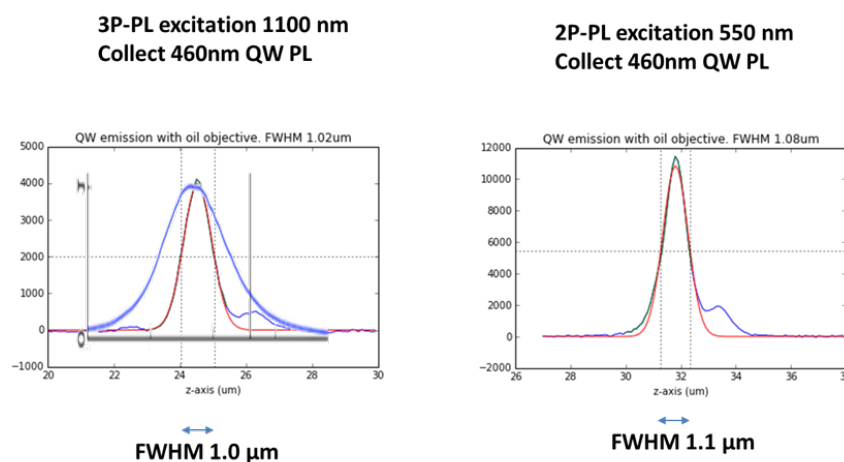


Figure T6.6. (Left) 3-photon PL excitation of quantum-well test sample. Original under-filled nominal depth resolution limited to 2.5 μm FWHM (thick blue curve). Fill-objective yields a 1.0 μm FWHM nominal depth resolution. (Right) Similarly, two photon excitation with a 550nm laser, yields a 1.1 μm FWHM nominal depth resolution.

Our goal in this to improve the depth resolution of 2P-TRPL to 1.0 μm . We found that due to aberrations and sample roughness, we were unable to achieve this result with custom solid immersion lens, as we had originally planned. However, using careful optimization of an oil-immersion system, we were able to achieve a nominal 1.0 μm depth resolution.

Conclusions

We have shown with this project that it is possible to use two-photon lifetime mapping of PV materials to gain new understanding of carrier dynamics that have previously been hidden below the surface of a film. Specifically, our work on CdTe has shown it is critical to separate surface recombination from TRPL measurements in order to extract bulk carrier lifetime. Additionally, we have found that sub-surface optoelectronic heterogeneity, specifically at grain boundaries in CdTe are critical to understand device performance. Neither of these conclusions would have been possible without high-resolution 3D mapping made possible with the 2P-TRPL technique developed in this project.

This work demonstrates a well-defined method to quantify grain-boundary, interface, and bulk recombination in CdTe and other optically-active polycrystalline semiconductor materials. Future efforts to develop detailed, accurate models will be able to extract surface, interface, grain-boundary, and bulk recombination rates throughout such polycrystalline films. This information can provide critical information to the development of next-generation photovoltaics and many other semiconductor technologies.

The development of high-resolution 3D two-photon microscopy for photovoltaics has been received with great interest to the PV community. Our microscopy system is now available for collaboration at the Molecular Foundry, a DOE User Facility, that allows scientists from around the world have access to this technique. We have had numerous discussion for collaborations on a wide variety of PV materials. Many of these discussions have evolved into active user projects at the Molecular Foundry. In addition, we have presented this work at numerous international conferences and have created two papers based on this work, one currently published, and one in preparation:

- Barnard, E. S. *et al.* Probing carrier lifetimes in photovoltaic materials using subsurface two-photon microscopy. *Sci. Rep.* **3**, (2013).
- Edward S. Barnard, Benedikt Ursprung, Eric Colegrove, Helio R. Moutinho, Nicholas J. Borys, Brian E. Hardin, Craig H. Peters, Wyatt K. Metzger, P. James Schuck. High-resolution three-dimensional lifetime tomography of CdTe photovoltaic devices. *In Preparation*.

At the end of the project were able to achieve all the stated milestones of this project. At the go/no-go point we had challenges with the depth resolution milestone, so Task 6 was added to address it. We subsequently were able to demonstrate the depth resolution milestone in that task, completing all requirements of this project.

Budget and Schedule

The start and end dates for the grant period are shown in the table below. The original budget and actual spend for both the federal and non-federal portions are also shown in the table below. Included in the federal portion of \$450,000 is \$105,000 that was paid to Dr. Shaul Aloni of the Molecular Foundry, an FFRDC. This money was passed through PLANT PV to this FFRDC and was therefore not part of the amount used to calculate the cost share. This means that \$345,000 was paid to PLANT PV for work performed under this grant. PLANT PV spent \$86,250 toward this grant, which represents a 20% cost share.

Calendar Quarter	Year	From	To	A. Federal Share Initial Plan	B. Federal Share Updated Actuals & Plan	Cumulative Federal Share	C. Recipient Share Initial Plan	D. Recipient Share Updated Actuals & Plan	Cumulative Recipient Share		
Q4	2012	10/1/2012	12/31/2012	\$35,008.67	\$35,008.67	\$35,008.67	\$6,252.16	\$6,252.17	\$6,252.17		
Q1	2013	1/1/2013	3/31/2013	\$58,186.59	\$39,276.44	\$74,285.11	\$12,359.14	\$6,955.62	\$13,207.79		
Q2	2013	4/1/2013	6/30/2013	\$42,890.10	\$33,379.61	\$107,664.72	\$8,535.02	\$6,040.21	\$19,248.00		
Q3	2013	7/1/2013	9/30/2013	\$37,663.59	\$24,565.85	\$132,230.57	\$7,228.38	\$2,832.58	\$22,080.58		
Q4	2013	10/1/2013	12/31/2013	\$34,575.89	\$30,485.94	\$162,716.51	\$6,456.47	\$5,473.59	\$27,554.17		
Q1	2014	1/1/2014	3/31/2014	\$32,093.59	\$54,804.36	\$217,520.87	\$6,148.39	\$13,701.09	\$41,255.26		
Q2	2014	4/1/2014	6/30/2014	\$33,343.59	\$31,361.84	\$248,882.71	\$6,148.39	\$7,840.46	\$49,095.72		
Q3	2014	7/1/2014	9/30/2014	\$38,543.59	\$23,435.24	\$272,317.95	\$7,448.40	\$5,858.81	\$54,954.53		
Q4	2014	10/1/2014	12/31/2014	\$37,663.59	\$24,110.68	\$296,428.63	\$7,228.40	\$6,027.67	\$60,982.20		
Q1	2015	1/1/2015	3/31/2015	\$33,343.59	\$46,605.23	\$343,033.86	\$6,148.39	\$7,047.46	\$68,029.66		
Q2	2015	4/1/2015	6/30/2015	\$33,343.59	\$50,499.16	\$393,533.02	\$6,148.38	\$7,054.58	\$75,084.24		
Q3	2015	7/1/2015	9/30/2015	\$33,343.62	\$46,334.05	\$439,867.07	\$6,148.48	\$9,565.27	\$84,649.51		
Q4	2015	10/1/2015	12/31/2015	\$0.00	\$10,132.93	\$450,000.00	\$0.00	\$1,600.49	\$86,250.00		
Totals				\$450,000.00	\$450,000.00		\$86,250.00	\$86,250.00			
				Updated Federal Spend Plan matches the baseline.						Updated Recipient Spend Plan matches the baseline.	

Path Forward

This project has a strong path forward at the conclusion of the funding period. We have created a unique characterization capability that is now part of a Department of Energy user facility, the Molecular Foundry (MF). Recently a number of MF user projects using 2P-TRPL have been approved. They include groups from NREL, University of Illinois Chicago, MIT, and the Colorado School of Mines. In addition, we are in discussions to establish industrial collaborations with First Solar Inc. and Stion Inc. We anticipate many fruitful results, including peer-reviewed publications, from these diverse set of collaborations. For example, our collaboration with Metzger's group at NREL will continue as we explore how novel processing and doping techniques effect CdTe efficiency and local carrier recombination dynamics.

This method has the possibility to be used as a research tool for both academic and industry photovoltaic scientists, as evidenced by our numerous collaborations. With appropriate sample preparation and optics, solid immersion lens technology has the possibility to push resolution limits of this technique to sub-micron levels, enabling a new class of measurements on ultra thin film PV materials. Additionally, it is possible for 2P-TRPL mapping to be used in a limited role as an inline tool for quality control in manufacturing, but throughput challenges would need to be overcome.

References

- Ahrenkiel, R. K., Call, N., Johnston, S. W. & Metzger, W. K. Comparison of techniques for measuring carrier lifetime in thin-film and multicrystalline photovoltaic materials. *Sol. Energy Mater. Sol. Cells* **94**, 2197–2204 (2010).
- Metzger, W. K. *et al.* Time-resolved photoluminescence studies of CdTe solar cells. *J. Appl. Phys.* **94**, 3549–3555 (2003).
- Metzger, W. K., Repins, I. L. & Contreras, M. A. Long lifetimes in high-efficiency Cu(In,Ga)Se₂ solar cells. *Appl. Phys. Lett.* **93**, 022110 (2008).
- Nelson, R. J. & Sobers, R. G. Interfacial recombination velocity in GaAlAs/GaAs heterostructures. *Appl. Phys. Lett.* **32**, 761–763 (1978).
- Shimakawa, S. *et al.* Characterization of Cu(In,Ga)Se₂ thin films by time-resolved photoluminescence. *Phys. Status Solidi A* **203**, 2630–2633 (2006).

6. BAŞOL, B. M. PROCESSING HIGH EFFICIENCY CdTe SOLAR CELLS. *Int. J. Sol. Energy* **12**, 25–35 (1992).
7. Dharmadasa, I. Review of the CdCl₂ Treatment Used in CdS/CdTe Thin Film Solar Cell Development and New Evidence towards Improved Understanding. *Coatings* **4**, 282–307 (2014).
8. McCandless, B. E., Moulton, L. V. & Birkmire, R. W. Recrystallization and sulfur diffusion in CdCl₂-treated CdTe/CdS thin films. *Prog. Photovolt. Res. Appl.* **5**, 249–260 (1997).
9. Moutinho, H. R. *et al.* Studies of recrystallization of CdTe thin films after CdCl₂ treatment. in *CONFERENCE RECORD IEEE PHOTOVOLTAIC SPECIALISTS CONFERENCE* **26**, 431–434 (1997).
10. Li, C. *et al.* Grain-Boundary-Enhanced Carrier Collection in CdTe Solar Cells. *Phys. Rev. Lett.* **112**, 156103 (2014).
11. Durose, K. *et al.* Key Aspects of CdTe/CdS Solar Cells. *Phys. Status Solidi B* **229**, 1055–1064 (2002).
12. Visoly-Fisher, I., Cohen, S. R., Gartsman, K., Ruzin, A. & Cahen, D. Understanding the Beneficial Role of Grain Boundaries in Polycrystalline Solar Cells from Single-Grain-Boundary Scanning Probe Microscopy. *Adv. Funct. Mater.* **16**, 649–660 (2006).
13. Helmchen, F. & Denk, W. Deep tissue two-photon microscopy. *Nat Meth* **2**, 932–940 (2005).
14. Schuck, P. J., Grober, R. D., Roskowski, A. M., Einfeldt, S. & Davis, R. F. Cross-sectional imaging of pendeo-epitaxial GaN using continuous-wave two-photon microphotoluminescence. *Appl. Phys. Lett.* **81**, 1984–1986 (2002).
15. Serrels, K. A., Ramsay E., Warburton R. J. & Reid D. T. Nanoscale optical microscopy in the vectorial focusing regime. *Nat Photon* **2**, 311–314 (2008).
16. Barnard, E. S. *et al.* Probing carrier lifetimes in photovoltaic materials using subsurface two-photon microscopy. *Sci. Rep.* **3**, (2013).
17. Ma, J. *et al.* Dependence of the Minority-Carrier Lifetime on the Stoichiometry of CdTe Using Time-Resolved Photoluminescence and First-Principles Calculations. *Phys. Rev. Lett.* **111**, 067402 (2013).
18. Kuciauskas, D. *et al.* Charge-carrier transport and recombination in heteroepitaxial CdTe. *J. Appl. Phys.* **116**, 123108 (2014).
19. van de Nes, A., Billy, L., Pereira, S. & Braat, J. Calculation of the vectorial field distribution in a stratified focal region of a high numerical aperture imaging system. *Opt. Express* **12**, 1281–1293 (2004).
20. Ahrenkiel, R. K. & Johnston, S. W. An optical technique for measuring surface recombination velocity. *Sol. Energy Mater. Sol. Cells* **93**, 645–649 (2009).
21. Marsh, P., Burns, D. & Girkin, J. Practical implementation of adaptive optics in multiphoton microscopy. *Opt. Express* **11**, 1123 (2003).
22. Richardson, W. H. Bayesian-Based Iterative Method of Image Restoration. *J. Opt. Soc. Am.* **62**, 55 (1972).
23. Lucy, L. B. An iterative technique for the rectification of observed distributions. *Astron. J.* **79**, 745 (1974).